Thermal-responsive activation of engineered bacteria to trigger antitumor immunity post microwave ablation therapy

Yumin Wu[1,4], Bo Liu[1,4], Yifan Yan[1,4], Chuntao Gong[2], Kaiwei Wang[3], Nanhui Liu[1], Yujie Zhu[1], Maoyi Li[1], Chunjie Wang[1], Yizhe Yang[1], Liangzhu Feng ®[1] ✉ & Zhuang Liu ®[1] ✉

Incomplete tumor removal after microwave ablation (MWA), a widely used hyperthermia-based therapy, can result in tumor recurrence. Herein, attenuated Salmonella typhimurium VNP20009 is engineered to release interleukin-15&interleukin-15-receptor-alpha (IL-15&IL-15Rα) in response to mildly elevated temperature. Such 15&15R@VNP colonizes in tumors upon intravenous injection, and the expression of IL-15&IL-15Rα is triggered by MWA. Antitumor immune responses are elicited, efficiently suppressing tumor growth even after incomplete microwave ablation. We further design VNP20009 with thermal-responsive co-expression of both IL-15&IL-15Rα and soluble programmed cell death protein (sPD-1). Such sPD-1-15&15R@VNP can also reverse the functional suppression of immune cells driven by PD-1/PD-L1 axis, reinvigorating progenitor exhausted T cells, a critical subset of cytotoxic T lymphocytes responsive to immune checkpoint blockade. Such thermal-responsive engineered bacteria are thus a promising adjuvant therapy to potentiate tumor ablation therapies via effectively activating antitumor immunity.

Microwave ablation (MWA), along with other thermal ablation therapies such as radiofrequency ablation (RFA) or high-intensity focused ultrasound (HIFU), is a local treatment technique that utilizes heating to destruct tumor tissues[1]. In clinic, ablation therapies have been widely used to treat different types of solid tumors in various organs, as well as for the management of postoperative recurrence or residual small cancer nodules[2]. However, the rapid expansion of the ablation zone can lead to inadvertent ablation of adjacent tissues[3], preventing excessive ablation power especially when treating tumors nearby critical organs or large blood vessels. In the meanwhile, for tumors with large sizes and especially those with irregular shapes, incomplete tumor ablation often occurs, increasing the risks of tumor recurrence post ablations[4,5]. Therefore, there is a great need to develop an intervention that can amplify the therapeutic effects of ablation therapies

and prevent tumor recurrences in patients with tumors that cannot be completely ablated.

Boosting the activities of immune cells within the tumor microenvironment (TME) has emerged as a compelling strategy to augment the efficacy of tumor treatment[6]. Cytokines, due to their inherent potency and multifaceted immunomodulatory properties, have long been recognized as critical therapeutic targets in the field of immune oncology[7]. Interleukin (IL)-2, the first FDA-approved cytokine for metastatic renal cell carcinoma and advanced melanoma, expands NK and T cells but may also induce activation-induced cell death and Treg cell activation, while excessive levels in the TME can cause T cell exhaustion and reduced responsiveness to ICB therapy[8]. Partially sharing IL-2's receptor IL-2Rβ (CD122) and γc (CD132), IL-15, has gained significant attention due to its lower

[1]Jiangsu Key Laboratory for Carbon-Based Functional Materials & Devices, Institute of Functional Nano & Soft Materials (FUNSOM), Soochow University, Suzhou 215123 Jiangsu, China. [2]InnoBM Pharmaceuticals, Suzhou 215123 Jiangsu, China. [3]College of Pharmaceutical Sciences, Soochow University, Suzhou 215123, China. [4]These authors contributed equally: Yumin Wu, Bo Liu, Yifan Yan. ✉e-mail: lzfeng@suda.edu.cn; zliu@suda.edu.cn

induction of endothelial-related toxicity and weaker regulatory T cells (Tregs) stimulation activity[9]. This cytokine assumes a pivotal role in the development, homeostasis, activation, and survival of T cells and natural killer (NK) cells[10]. IL-15 exhibits a unique mode of action known as trans-presentation by forming a stable heterodimeric complex with its high-affinity receptor subunit, Interleukin-15-receptor-alpha (IL-15Rα)[11]. This complex is then trans-presented to T cells and NK cells to engage with the βγc receptor present in those cells[12,13]. Recent studies have elucidated the indispensable role of IL-15 within the TME in orchestrating optimal anti-tumor immune responses. In particular, IL-15 is able to sustain the activity of progenitor-exhausted CD8+ T cells (CD8 Tpex)[14], which are responsible for the antitumor therapeutic responses of immune checkpoint blockade (ICB) therapies targeting programmed cell death 1 (PD-1) or programmed death-ligand 1 (PD-L1)[15]. Various forms of IL-15, such as IL-15/IL-15Rα complexes and IL-15 muteins, have been developed to counteract immune suppression in preclinical and clinical studies[16,17]. However, the clinical progress of cytokines as cancer therapeutics has been hampered by their notable toxicities typically associated with systemic administration[18]. Conversely, local administration often requires multiple injections to achieve the desired therapeutic effect due to the rapid diffusion of proteins[19,20]. Therefore, it would be of great interest to design innovative strategies for continuous in situ generation of intratumoral IL-15, particularly in combination with IL-15Rα, to achieve sustained anti-tumor effects.

Bacteria, such as anaerobes or facultative anaerobes, have emerged as a prominent player in the field of tumor treatment, owing to their inherent characteristics of hypoxia tropism, which allows them to naturally colonize in immune-privileged tumors upon systemic administration, and thrive within hypoxic and necrotic TME[21,22]. Furthermore, by gene engineering, intelligent microbial delivery systems have recently been developed for therapeutic applications, enabling

them to activate gene expression under specific conditions[23,24]. Unlike chemical inducers, which are unable to target specific anatomical sites[25,26], and light-induced control elements, which suffer from limited penetration[27], thermal-responsive control elements can provide spatiotemporal control at varying depths[28,29].

Here, based on VNP20009, an attenuated *Salmonella typhimurium* strain with in vivo safety proven in a phase I clinical trial[30,31], we design thermal-sensitive engineered bacteria that can express IL-15&IL-15Rα in responsive to elevated temperature. The obtained engineered bacteria, named 15&15R@VNP, being silent under the body temperature (37 °C), would be turned on to initiate the expression of IL-15&IL-15Rα upon heating to above 42 °C. As a type of facultative anaerobic bacteria, such 15&15R@VNP upon intravenous injection would selectively colonize in the tumor. MWA treatment is then conducted to heat those tumors, not only eradicating tumor cells to facilitate the release of tumor antigens, but also triggering in situ generation of IL-15&IL-15Rα by bacteria to further activate anti-tumor immune responses. As a result, effective suppression of tumors with incomplete MWA could be achieved. To further alleviate immune suppression of tumors, VNP20009 with thermal-responsive co-expression of both IL-15&IL-15Rα and soluble PD-1 (sPD-1) is then designed to enable both immune stimulation and ICB, thereby enhancing the efficacy of Tpex and resulting in further improved therapeutic outcome (Fig. 1). Additionally, in an orthotopic liver cancer model, we observed improved outcome in rats treated with MWA combined with sPD-1-15&15R@VNP, highlighting the potent antitumor effects of our design. Moreover, safety evaluations demonstrate the safety profile of our therapeutic strategy with engineered bacteria. Consequently, our engineered thermal-responsive bacteria, in the context of MWA, could enable the integration of hyperthermia, immune response amplification, and ICB to boost the efficacy of tumor ablation therapies.
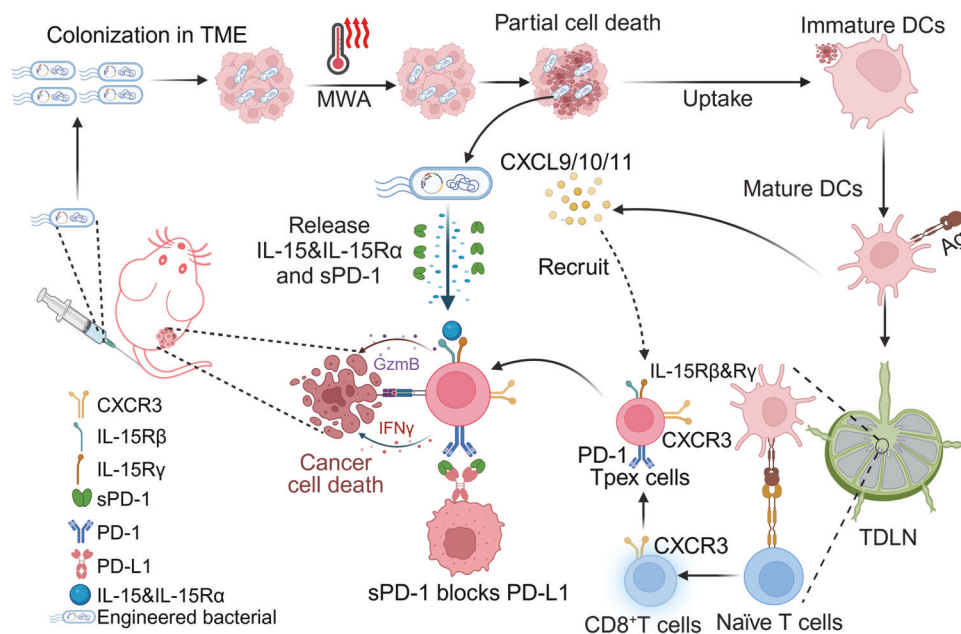

Fig. 1 | Schematic diagram of engineered bacteria to assist MWA cancer therapy. The tumor-specific colonization capability of engineered bacteria allows their significant accumulation in tumor tissues, exploiting the immunodeficiency and hypoxia of the tumor microenvironment, which facilitates their proliferation. Under the influence of MWA, a fraction of tumor cells would undergo cell death to release tumor antigens, which are then engulfed by DCs for antigen presentation. Those matured DCs would migrate to the TDLNs, where they educate naïve T cells and promote their differentiation into CD8+ T effector T cells. As a result of sustained antigen stimulation, a subset of these cells would be differentiated into Tpex cells. Meanwhile, activated DCs release CXCL9/10/11, which subsequently recruits these Tpex cells to infiltrate into the TME. Moreover, under the induction of MWA, engineered bacteria release IL-15&IL-15Rα and sPD-1. While IL-15&IL-15Rα plays a crucial role in maintaining the activity of Tpex cells and promoting their cytotoxicity against tumor cells, sPD-1 would reinvigorate Tpex cells, thereby facilitating the continuous process of T cell-specific killing of tumor cells. The figure was created in BioRender. (Yujie (2024) https://BioRender.com/l27u027).
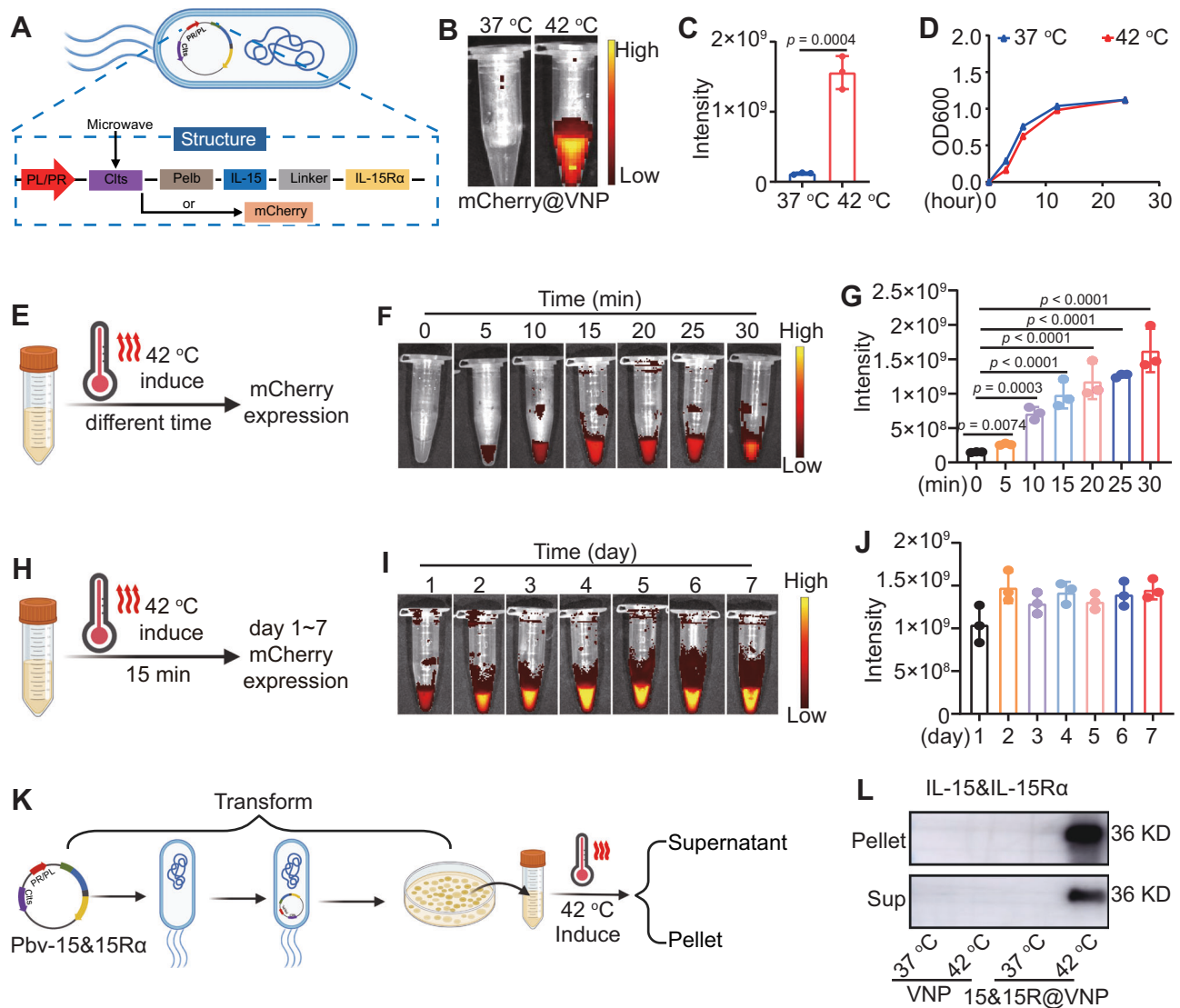
Fig. 2 | The hyperthermia induced gene expression by engineered bacteria.
A The scheme of the expression of IL-15&IL-15Rα or mCherry protein in engineered bacteria under hyperthermia, the figure was created in BioRender. Yujie (2024) https://BioRender.com/x95f139. Fluorescence images (**B**) and quantitative analysis (**C**) of mCherry fluorescence in mCherry@VNP under different temperature conditions ($n = 3$ samples, p value was calculated by the two-tailed Student's t test). **D** The growth activity of engineered bacteria after treatment under different temperatures, as indicated by OD_{600} ($n = 3$ samples). Scheme (**E**, the figure was created in BioRender. Yujie (2024) https://BioRender.com/k68x589), fluorescence image (**F**), and quantitative analysis (**G**) of mCherry in mCherry@VNP after heat induction for different durations ($n = 3$ samples, p values were calculated by one-

way ANOVA with Tukey's multiple comparisons). Scheme (**H**, the figure was created in BioRender. Yujie (2024) https://BioRender.com/r04v960), fluorescence image (**I**), and quantitative analysis (**J**) of mCherry in mCherry@VNP at different time points after 15 min of heat induction ($n = 3$ samples). Scheme (**K**, the figure was created in BioRender. Yujie (2024) https://BioRender.com/k18d759) and western blot images (**L**) of IL-15&IL-15Rα protein in bacterial pellets and induced supernatants of 15&15R@VNP under different temperature conditions, this experiment was repeated for three times independently with similar results. Data in **C**, **D**, **G**, and **J** were presented as mean ± SD. Sup supernatant. Source data are provided as a Source Data file.

Results

Engineering of thermal-responsive bacteria

To develop a thermal-responsive recombinant plasmid vector, we chose the pBV220 plasmid vector as the target for modification. This vector utilizes the leftward (PL) and rightward (PR) phage lambda promoters, which are commonly used in prokaryotic expression vectors for producing recombinant proteins and peptides[32]. Transcription from either promoter or both in tandem is repressed in prokaryotic cells growing at low temperatures (28–30 °C) by the thermolabile cI857 repressor expressed from the same vector. However, a temperature shift to 42–45 °C quickly inactivates the cI857 repressor, enabling the transcription of the inserted genes under the promoters and facilitating the overproduction of their encoded recombinant proteins[33].

To facilitate convenient verification and tracking, we initially constructed a prokaryotic recombinant plasmid vector pBV-mCherry by inserting a mCherry fluorescent reporter gene into the pBV220 plasmid vector (Fig. 2A). The successful construction of the recombinant plasmid vector was confirmed through restriction enzyme digestion and DNA gel electrophoresis (Supplementary Fig. 1A). Subsequently, the recombinant plasmid vector was transformed into attenuated *Salmonella typhimurium* strain VNP20009 to prepare the thermal-responsive bacterium mCherry@VNP (Fig. 2A). It was observed that incubating mCherry@VNP at 37 °C failed to elicit any detectable fluorescence signals, suggesting the suppressed expression of the mCherry fluorescent gene at this temperature. Conversely, strong red fluorescent signals emitted from bacteria became evident

when the incubation temperature was raised to 42 °C, while maintaining the viability of bacteria (Fig. 2B–D). Similarly, the engineered bacteria were subjected to varying durations of heating at 42 °C. The results demonstrated that within the range of 5 to 30 min, fluorescent emissions from the bacteria were observable (Fig. 2E–G). Subsequently, to validate the sustainability of engineered bacteria protein expression, we continuously monitored the fluorescence of bacteria after subjecting them to a 15-min heating period. As anticipated, the fluorescence of the engineered bacteria persisted until day 7 (Fig. 2H–J), indicating that a single initiation of the engineered bacteria would trigger continuous protein expression.

IL-15&IL-15Rα complex, with its superior capacity to sustain the functionality of NK cells and CD8+ T cells, has emerged as a prominent anti-tumor factor. To initiate our study, a murine tumor model was established using CT26 colon cancer cells to investigate the effects of intratumoral administration of the IL-15 and IL-15Rα complex on tumor growth. Notably, the results demonstrated a significant inhibition of tumor progression (Supplementary Fig. S2), providing compelling evidence for the potent antitumor activity of the IL-15 and IL-15Rα complex. Since the fusion of IL-15 and IL-15Rα structural domains using a linker molecule has demonstrated notably augmented effects as opposed to IL-15 plus IL-15Rα structural domains[34], the mCherry gene in pBV-mCherry was replaced by the murine IL-15&IL-15Rα fused using a flexible linker to maintain proper connectivity and conformational integrity. Moreover, to facilitate the secretion of IL-15&IL-15Rα, a Pelb signal peptide has been introduced and placed at the N-terminus of IL-15&IL-15Rα (Fig. 2A)[35]. The presence of the IL-15&IL-15Rα gene fragment in the plasmid was verified through agarose gel electrophoresis (Supplementary Fig. 1B). Similarly, the recombinant plasmid vector was transformed into attenuated *Salmonella typhimurium* strain VNP20009 to prepare thermal-responsive bacterium 15&15R@VNP. Moreover, the protein expression of IL-15&IL-15Rα in the thermal-responsive bacteria 15&15R@VNP was detected under different temperatures at 37 and 42 °C. As expected, robust expression of IL-15&IL-15Rα by such bacteria was found under the induction condition at 42 °C, whereas no detectable leakage expression was observed under the physiological temperature at 37 °C (Fig. 2K, L). Similarly, the engineered 15&15R@VNP were subjected to heating at 42 °C for 30 min. The results demonstrated a significant increase in the protein content secreted into the culture supernatant when comparing the engineered bacteria cultured at 37 °C for an additional 6 h post-induction to those assessed immediately after the 30-min induction (Supplementary Fig. 3A). This suggested that heat-activated bacteria could continuously produce the protein at 37 °C. Next, the engineered 15&15R@VNP were subjected to varying durations of heating at 42 °C. The results demonstrated that with prolonged incubation time, the expression levels of IL-15&IL-15Rα gradually increased (Supplementary Fig. 3B). Finally, the activity of IL-15&IL-15Rα to stimulate T-cell proliferation was also successfully verified (Supplementary Fig. 4). Collectively, we developed engineered bacteria that remain dormant at physiological temperatures but undergo activation to effectively secrete functional proteins under high-temperature conditions.

MWA-triggered protein expression by engineered bacteria post intravenous injection

The attenuated *Salmonella typhimurium* strain, VNP20009, like other types of anaerobes, is known to be able to colonize within solid tumors upon intravenous (i.v.) injection. Unlike in normal tissues where these attenuated bacteria are cleared, the diminished immune surveillance within hypoxic tumor tissues allows them to proliferate within the TME[36]. To evaluate the tumor-targeting efficacy of the bacteria, engineered bacteria were intravenously administered into H22 tumor-bearing mice. At different time points, various tissues were collected, homogenized, and subsequently plated onto LB culture plates to evaluate bacteria colonies (Fig. 3A). Although residual bacteria were observed in normal tissues within at early time points post-injection, nearly complete eradication of bacteria colonies in normal tissues were found after 72 h. In marked contrast, a substantial elevation in bacteria load was observed within tumors, exhibiting a 10,000-fold increase compared to healthy organs (Fig. 3B, C). Immunofluorescence staining assay confirmed that salmonella typhimurium showed high levels in the hypoxic regions of a tumor (overexpression of hypoxia-inducible factor alpha (HIF-1α)) (Supplementary Fig. 5). These results illustrated that the salmonella typhimurium could be efficiently accumulated in the tumor site and penetrated into the tumor hypoxic region. This finding strongly suggests the selective proliferation of VNP20009 within the TME. Similarly, complete clearance of bacteria in all examined organs was observed for healthy mice with i.v. injection of bacteria, with no risk of recurrence over day 30 (Supplementary Fig. 6A, B).

SDS-PAGE gel electrophoresis analysis revealed that 15&15Rα was present in the lysates of bacteria induced by MWA for 30 min, and was absent in the lysates of bacteria incubated at 37 °C (Supplementary Fig. 7). This finding confirms the successful production of therapeutic 15&15Rα following MWA treatment. Subsequently, the MWA treatment was carried out for H22-tumor-bearing mice 72 h following i.v. injection of engineered bacteria to assess the efficacy of MWA in inducing protein expression by the bacteria (Fig. 3D). The local tumor temperature was monitored using an infrared thermographic instrument, ensuring the maintenance of tumor temperatures within the range of 42–47 °C (Fig. 3E). As revealed by in vivo fluorescence imaging, for mCherry@VNP injected mice with their tumors post MWA treatment, strong red fluorescence was observed solely in the tumor but not in other organs (Fig. 3F). This observation confirms the feasibility of using MWA to induce the expression of specific proteins by our engineered thermal responsive bacteria colonized inside tumors post i.v. injection.

Next, a separate set of experiments was conducted in tumor-bearing mice to examine the possibility of using MWA to trigger IL-15&IL-15Rα expression in tumor tissue by 15&15R@VNP. To mimic the incomplete MWA that may occur in some clinical practices and would lead to unsatisfactory therapeutic performance, we selected an ablation temperature around 42–47 °C, a relatively mild temperature. Mice bearing H22 tumors were i.v. injected with 15&15R@VNP at a dose of 2×10^6 CFU/mouse. Following a 72-h interval, these mice were subjected to MWA therapy, while maintaining a consistent temperature around 42 °C to 47 °C during MWA. The IL-15&IL-15Rα concentrations in the tumor and peripheral blood were quantified at different time points (6 h, 12 h, 24 h, 3 days, and 7 days) following MWA treatment (Fig. 3G, H). Significantly increased IL-15&IL-15Rα levels were found in tumor tissue at 6 h post-MWA treatment, and persisted for 14 days, suggesting a sustained provision of IL-15&IL-15Rα within the TME by engineered bacteria. In marked contrast, tumors in mice with i.v. injection of 15&15R@VNP but in the absence of MWA treatment showed no significant increase in 15&IL-15Rα levels (Fig. 3I).

The clinical applications of cytokines as cancer therapeutics have been limited by their substantial toxicities associated with systemic administration[18]. Of significant importance, there was no discernible increase of IL-15&IL-15Rα in the peripheral blood for 15&15R@VNP injected tumor-bearing mice post MWA treatment (Fig. 3J), suggesting that the cytokine produced by tumor-colonized bacteria would be unlikely to cause systemic toxicity. Subsequently, blood cell and biochemical analyses were performed for those 15&15R@VNP injected tumor-bearing mice post-MWA treatment. The serum levels of aminotransferase (ALT) and aspartate aminotransferase (AST), which are markers for liver damage, were both found to be normal (Fig. 3K, L). Moreover, various blood cell-related parameters were also found to be in the normal ranges (Supplementary Fig. 8). Additionally, histological analysis of major organs including the heart, liver, spleen, lungs, and kidneys using Hematoxylin and eosin (H&E) staining revealed
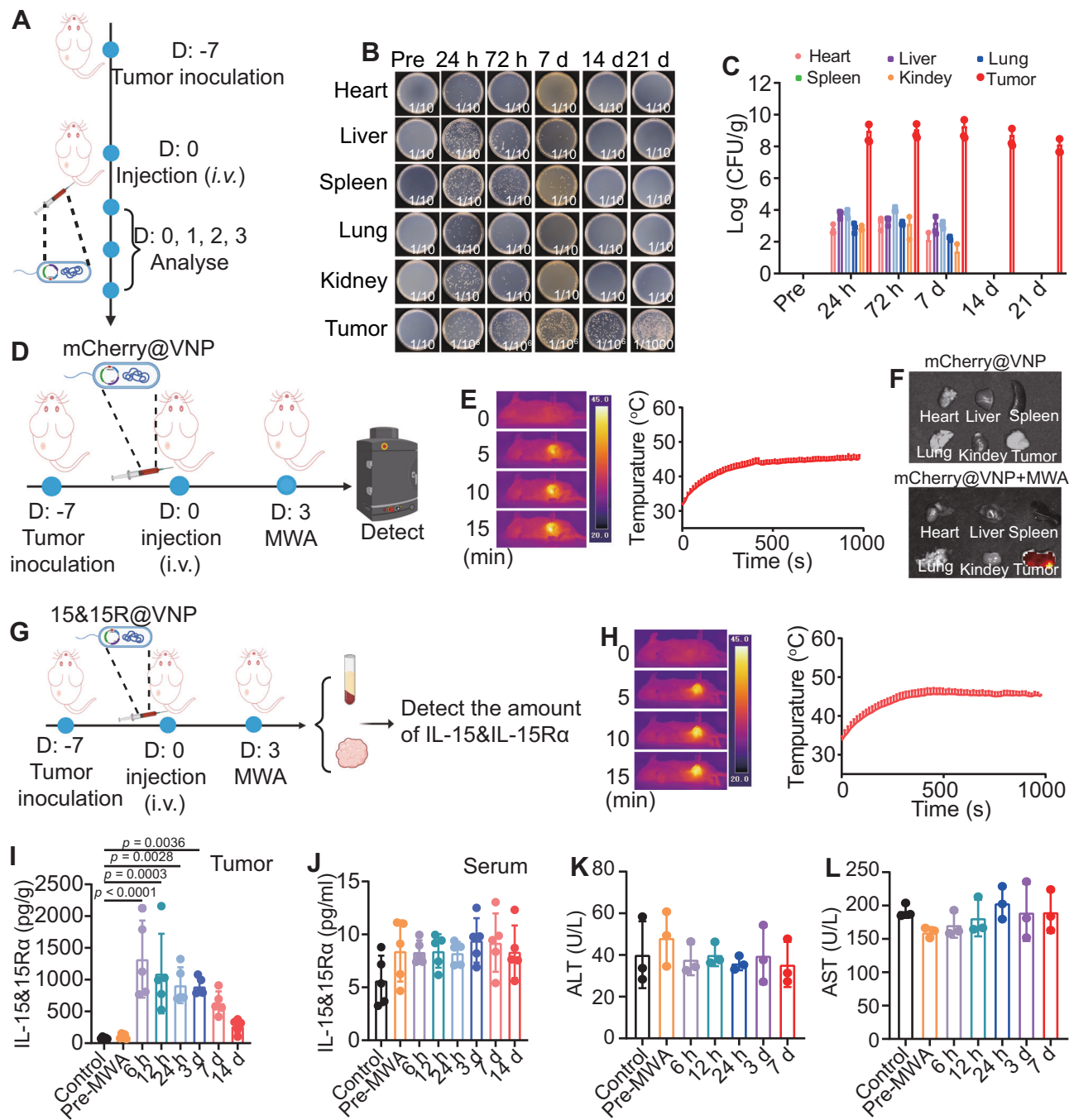
Fig. 3 | Tumor-specific colonization and MWA-induced protein expression by engineered bacteria. A Schematic illustration of tumor-specific colonization using engineered bacteria, the figure was created in BioRender. Yujie (2024) https://BioRender.com/j49y03l. Representative photographs (**B**) and quantification (**C**) of bacterial colonization in major organs and tumors obtained from H22 tumor bearing mice at different time points after intravenous administration of engineered bacteria (*n* = 3 mice). Schematic illustration (**D**, the figure was created in BioRender. Yujie (2024) https://BioRender.com/m99p797) and representative thermal images (left) and microwave heating profiles (right) (**E**) of tumor sites from mice post intravenous administration of mCherry@VNP in vivo (*n* = 3 mice). **F** Representative fluorescence imaging of MWA induction of the mCherry expression in multiple organs (*n* = 3 mice). **G** Schematic diagram of MWA induction of the IL-15&IL-15Rα expression in engineered bacteria in vivo, the figure was created in

BioRender. Yujie (2024) https://BioRender.com/r44b770. **H** Representative thermal images (left) and microwave heating profiles (right) of tumor sites from mice post intravenous administration of engineered bacteria (*n* = 5 mice). **I** Quantification of IL-15&IL-15Rα protein levels in tumor tissue homogenates at different time points following MWA in mice (*n* = 5 mice, *p* values were calculated by one-way ANOVA with Tukey's multiple comparisons). **J** Quantification of IL-15&IL-15Rα protein levels in peripheral serum at different time points following MWA in mice (*n* = 5). Quantification of ALT (**K**) and AST (**L**) protein levels in peripheral serum at different time points following MWA in mice (*n* = 3 mice). Data in **C**, **E**, **H**, and **I**–**L** were presented as the mean ± SD. CFU colony-forming units, MWA microwave ablation, ALT alanine transaminase, AST aspartate aminotransferase. Source data are provided as a Source Data file.

no risk of organ damage in tumor-bearing mice subjected to 15&15Ra and MWA treatments (Supplementary Fig. 9), further demonstrating the superior safety of our engineered bacteria colonized in the tumor even post activation by MWA treatment.

15&15R@VNP combined with MWA for in vivo tumor treatment

Encouraged by the aforementioned results, and MWA combined with VNP has also been shown to promote tumor control[37], we sought to explore the therapeutic efficacy of 15&15R@VNP combined with MWA in tumor-bearing mice. Given the prevalent use of MWA in the treatment of liver cancer[38], we opted to begin our study by employing a H22 mouse liver cancer model. Once the tumor volume reached approximately 100 mm³, the mice were randomly divided into six groups and treated as follows: group I (control) and group II (MWA) received PBS administration, group III (VNP) and group V (MWA + VNP) received VNP20009 treatment, group IV (15&15R@VNP) and group VI (MWA + 15&15R@VNP) received 15&15R@VNP treatment. After 3 days, MWA treatment was carried out for tumors in groups II, V, and VI (Fig. 4A). During MWA, the temperature of the tumor site was continuously monitored using an infrared thermometer, ensuring that it remained within the optimal range of 42–47 °C (Fig. 4B, C). Notably, we found that there was no significant change in the bacteria population within the tumor post-MWA (Supplementary Fig. 10), suggesting that MWA treatment at this mild condition would not significantly kill bacteria colonized in the tumor.

By monitoring the tumor growth, we found that compared to the control group (group I), MWA alone (group II) exhibited a negligible tumor suppression effect, which could be attributed to the moderate heating condition in our experiment. Additionally, in H22 tumor-bearing mice treated with VNP20009, irrespective of the presence of MWA, the tumor suppression was also not significant. In contrast, while H22 tumor-bearing mice treated with 15&15R@VNP (group IV) did not show any tumor suppression effect in the absence of MWA, 15&15R@VNP injection together with MWA treatment of tumors (group VI) could effectively suppress the tumor growth (Fig. 4D). Moreover, this therapeutic regimen demonstrated a remarkable extension in the survival duration of mice, with one out of five tumor-bearing mice achieved complete remission (CR) (Fig. 4E and Supplementary Fig. 11). Furthermore, through monitoring the body weight of mice in each group, we observed that even when MWA was utilized to induce the expression of IL-15&IL-15Rα in 15&15R@VNP (group VI), there was almost no change in the mouse body weight (Fig. 4F), supporting the safety of the proposed therapeutic regimen. Notably, TdT-mediated dUTP nick-end labeling (TUNEL) staining and H&E staining further verified that mice in group VI exhibited the highest degree of tumor cell damage (Fig. 4G and Supplementary Fig. 12), evidencing the significant therapeutic effect of 15&15R@VNP in combination with MWA on tumors.

Subsequently, an identical set of experimental procedures was replicated for the CT26 colorectal cancer model to determine the therapeutic efficacy of MWA in combination with 15&15R@VNP (Fig. 4H). As expected, mice bearing CT26 tumors with 15&15R@VNP injection and MWA treatment (group VI) showed the most significant tumor suppression, as compared to the other groups (Fig. 4I). Notably, this combination therapy resulted in a significant extension in the overall survival of mice, reaching a CR rate of three out of six. (Fig. 4J, K). Furthermore, during a 60-day observation period, no tumor recurrence was observed. Additionally, the minimal fluctuation in body weight among the mice further attests to the safety of this treatment regimen (Supplementary Fig. 13).

Immune responses triggered by engineered bacteria in assisting MWA therapy

Next, we further investigated the underlying mechanisms of 15&15R@VNP in assisting MWA treatment. Subsequently, we proceeded to establish a H22 tumor-bearing mouse model and replicated the experimental protocol employed in our previous study. On the third day post-MWA treatment, mice from each experimental group were euthanized, with their tumor tissues, tumor-draining lymph nodes (TDLNs), and peripheral blood samples collected for subsequent analysis (Fig. 5A). By analyzing the maturation of DCs within TDLNs, we observed a significant increase in the proportion of mature DCs when MWA and bacteria were present simultaneously (Supplementary Fig. 14).

Next, we further investigated the activation of the intratumoral immune responses following the treatment. Importantly, when compared to the other groups, the combined treatment group (group VI) exhibited a remarkable increase in the proportion of CD8⁺ T cells (CD45⁺CD3⁺CD8⁺) within the tumor tissues of mice (Fig. 5B, C). Meanwhile, the observed increase in the presence of Ki67⁺CD8⁺ T cells (CD45⁺CD3⁺CD8⁺Ki67⁺), as well as activated T cells (CD69⁺ T cells, CD45⁺CD3⁺CD69⁺) and activated CD8⁺ T cells (CD69⁺CD8⁺ T cells, CD45⁺CD3⁺CD8⁺CD69⁺) further supported the effects of IL-15&IL-15Rα expressed by 15&15R@VNP in enhancing T cell responses (Fig. 5D–F and Supplementary Fig. 15A–C). Nevertheless, no substantial alteration was observed in the quantity of CD4⁺ T cells (Fig. S16). This could be attributed to the predominant role of CD8⁺ T cells in mediating the anti-tumor immune responses. However, whether there are alterations in CD4⁺ T cell subsets, as well as the dynamics among different CD4⁺ T cell subsets, will be the focus of our subsequent investigations[39]. Furthermore, mice in the combined treatment group (group VI) showed a notable increase in NK cell proportion within tumor tissues compared to other experimental groups (Supplementary Fig. 17). This increase was accompanied by a higher percentage of activated NK cells (CD69⁺ NK cells, CD45⁺CD3⁻CD49b⁺CD69⁺) in the combined treatment group (group VI), indicating the potent effect of IL-15&IL-15Rα in promoting NK cell activation (Fig. 5G and Supplementary Fig. 15D).

As a critical cytokine involved in the elimination of tumor cells within the TME, IFN-γ is primarily secreted by CD8⁺ T cells. Consequently, we assessed the proportion of IFN-γ-secreting CD8⁺ T cells (IFN-γ⁺CD8⁺ T cells, CD45⁺CD3⁺CD8⁺IFN-γ⁺) and observed a significant increase in the proportion of these cells within the tumors of mice treated with combined treatment (group VI) compared to mice in other groups (Fig. 5H, I). This finding underscores the ability of 15&15R@VNP to effectively sustain IFN-γ secretion in CD8⁺ T cells. This was further confirmed by the elevated protein levels of IFN-γ in the tumor tissues of mice receiving combined treatment (group VI) compared to mice in other groups (Fig. 5J). Encouragingly, no discernible increase in IFN-γ levels was observed in the peripheral blood of mice in the combined treatment group (group VI) compared to the other experimental groups (Fig. 5K).

Although these results are indeed highly exciting, it is important to note that the persistent exposure of T cells to antigens and continuous stimulation of the T-cell receptor (TCR) may potentially result in a progressive functional decline and subsequent exhaustion of T cells[40]. This exhaustion is often characterized by the upregulation of PD-1 expression. Consequently, we comprehensively assessed T cell exhaustion in the tumor tissues of different mouse cohorts. Our findings revealed a significant increase in the proportion of PD-1⁺CD8⁺ T cells in mice treated with combined treatment (group VI), compared to the other experimental groups (Fig. 5L, M and Supplementary Fig. 18).

Our immunological evaluation analysis mentioned above has confirmed that the anti-tumor immune responses triggered by the combined MWA with 15&15R@VNP primarily relies on CD8⁺ T cells and NK cells. Next, a set of animal experiments was performed utilizing the H22 tumor model, wherein CD8⁺ T cells and NK cells were depleted by corresponding antibodies. As shown in the Fig. 5N, once the tumor volume reached approximately 100 mm³, the mice were randomly divided into five groups. Specifically, with group I receiving PBS
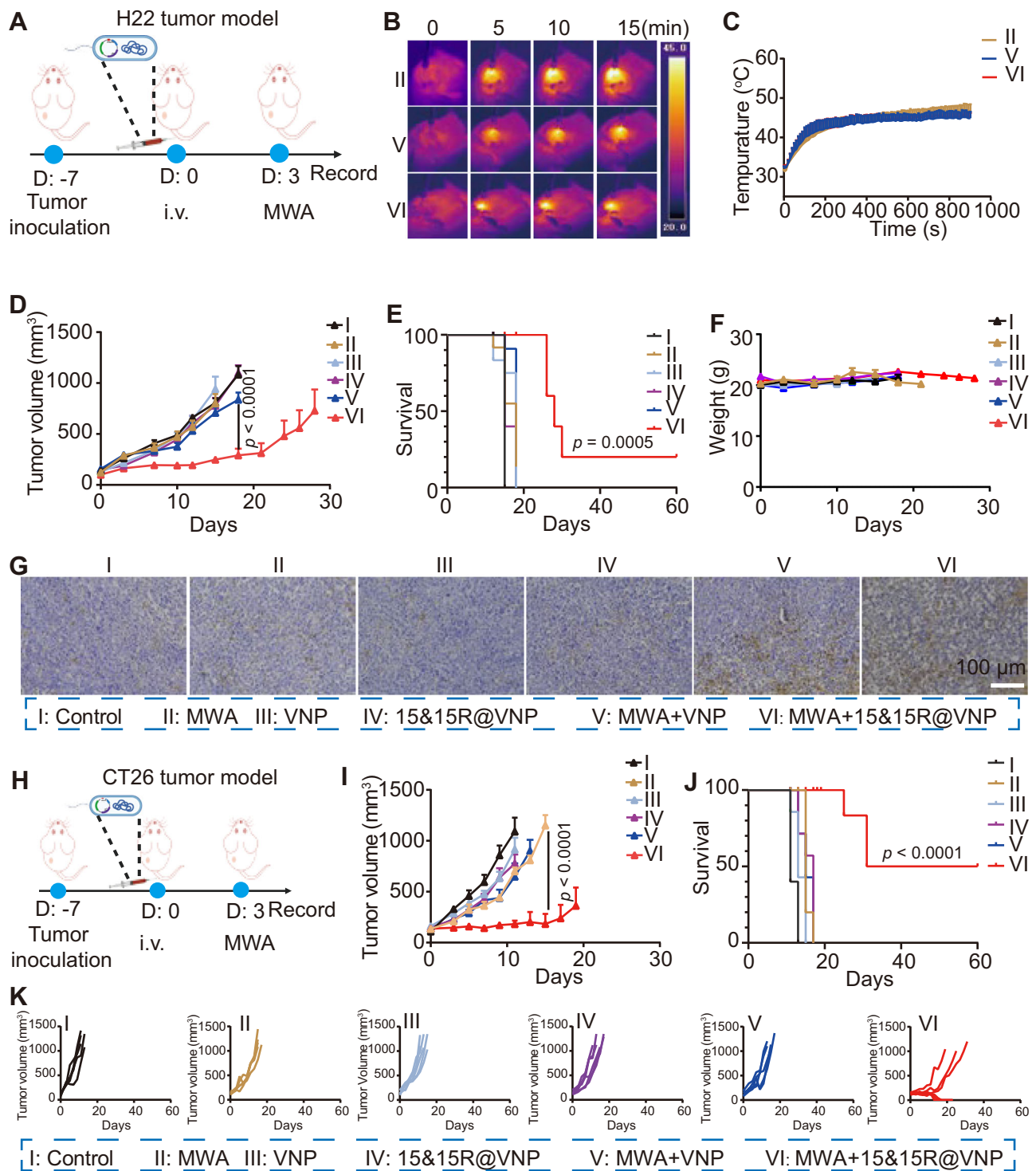
Fig. 4 | Synergistic therapeutic efficacy of 15&15R@VNP combined with MWA.
A Schematic illustration of the in vivo treatment schedule using a murine H22 tumor model, the figure was created in BioRender. Yujie (2024) https://BioRender.com/y24m952. Representative thermal images (**B**), and corresponding microwave heating profiles (**C**) of mice after different treatments as indicated ($n = 3$ mice). Tumor curves (**D**, group I ($n = 7$ mice), group II, III, IV, and V ($n = 6$ mice), group VI ($n = 5$ mice)), corresponding mobility-free survival rate (**E**), average body weights (**F**), and magnified TUNEL staining images of tumor section (**G**) of mice after different treatments as indicated. The scale bar in **G** was 100 µm, the experiment in **G** was repeated for three times independently with similar results. **H** Schematic illustration of the in vivo therapeutic schedule using a murine CT26 tumor model, the figure was created in BioRender. Yujie (2024) https://BioRender.com/y24m952. Tumor growth curves (**I**, group I, III, IV, and VI ($n = 6$ mice), group II and V ($n = 5$ mice)), corresponding mobility-free survival rate (**J**), and individual tumor growth curves (**K**) of CT26 tumor-bearing mice after different treatments as indicated. Data in **C–F**, **I**, and **J** were presented as the mean ± SEM. The p values in **D** and **I** were calculated by two-way ANOVA with Tukey's multiple comparisons; The p values in **E** and **J** were calculated by the log-rank test. MWA microwave ablation. Source data are provided as a Source Data file.

I: Control   II: MWA   III: VNP   IV: 15&15R@VNP   V: MWA+VNP   VI: MWA+15&15R@VNP
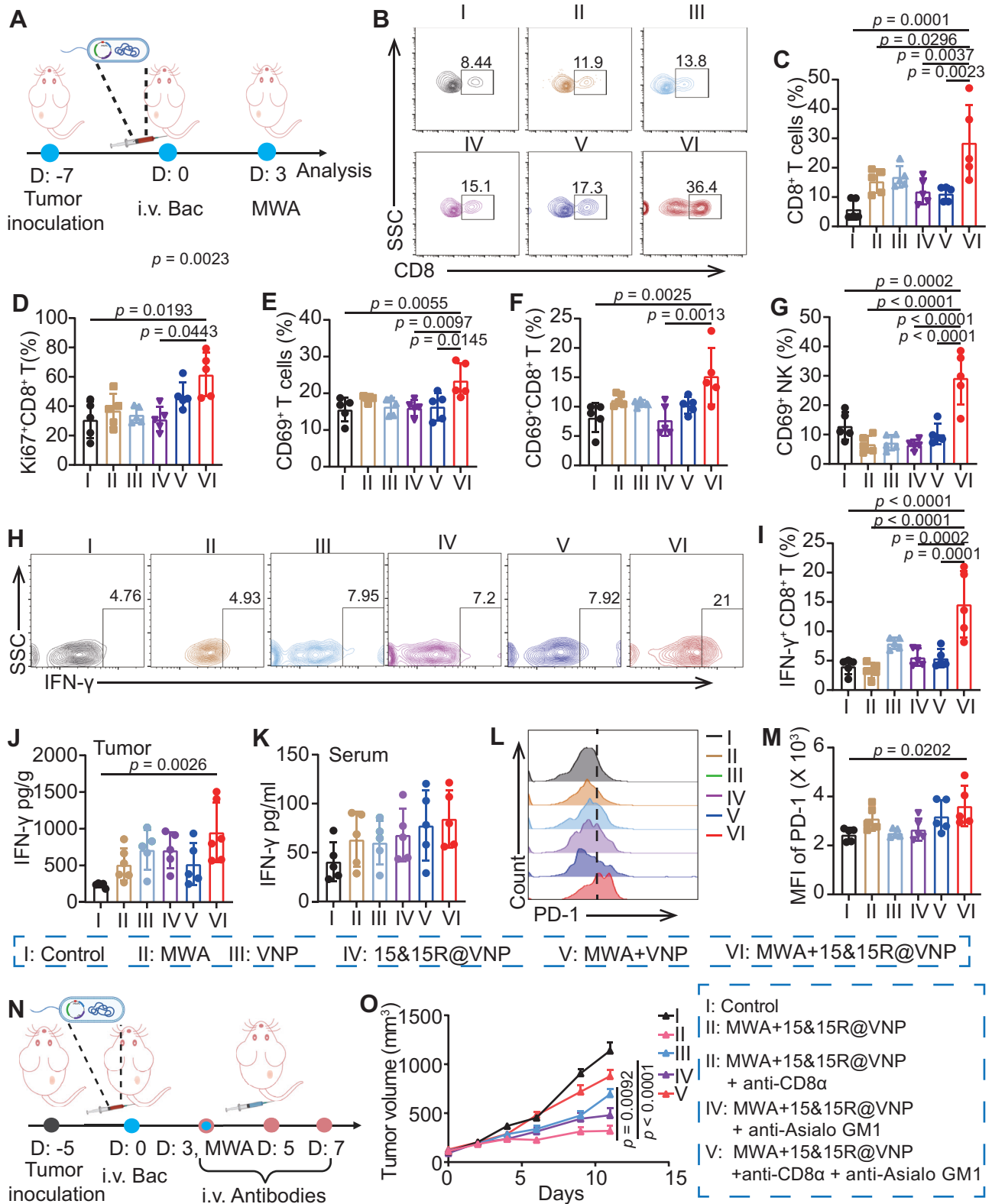
administration at the control, group II-V all received combined MWA and 15&15R@VNP treatment, together with intravenous injection of the control antibody anti-IgG (group II), anti-CD8α antibody to deplete CD8+ T cells (group III), anti-ASIO GM1 antibody to deplete NK cells (group IV), and anti-CD8α + anti-ASIO GM1 antibodies to simultaneously deplete both CD8+ T cells and NK cells (group V). The engineered bacteria were intravenously injected into the mice at day 0 with a dosage of 2×10^6 CFU per mouse. After 3 days, MWA treatment was

carried out in groups II, III, IV, and V, heat up the tumors to a temperature of around 42–47 °C. Anti-CD8α and anti-ASIO GM1 antibodies were administered intravenously on days 3, 5, and 7 at a dose of $1 \, \mathrm{mg \, kg^{-1}}$ per mouse, respectively. Notably, up simultaneous depletion of CD8+ T cells and NK cells, the tumor suppression effect by the combined MWA + 15&15R@VNP would no longer exist (Fig. 5O), while the single depletion of CD8+ T cells or NK cells partially interfered with the synergistic therapeutic effects. Our results demonstrate the

Fig. 5 | Mechanism study of 15&15R@VNP-assisted MWA therapy. A Schematic illustration of the in vivo mechanism study in a murine H22 tumor model, the figure was created in BioRender. Yujie (2024) https://BioRender.com/y24m952. Flow cytometric analysis (**B**) and proportions (**C**) of CD8^{+} T cells (CD45^{+}CD3^{+}CD8^{+}) in tumor tissues after different treatments as indicated. Proportions of Ki67^{+}CD8^{+} T cells (CD45^{+}CD3^{+}CD8^{+}Ki67^{+}, **D**), CD69^{+} T cells (CD45^{+}CD3^{+}CD69^{+}, **E**) and CD69^{+}CD8^{+} T cells (CD45^{+}CD3^{+}CD8^{+}CD69^{+}, **F**) inside the tumors after various treatments as indicated. **G** Intratumoral percentages of CD69^{+} NK cells (CD45^{+}CD3^{−}CD49b^{+}CD69^{+}) after different treatments as indicated. Flow cytometric analysis (**H**) and proportions (**I**) of IFN-γ^{+} T cells (CD45^{+}CD3^{+}CD8^{+}IFN-γ^{+}) in tumor tissues after different treatments as indicated. The protein levels of IFN-γ inside the tumors (**J**) and in serum (**K**) after various treatments as indicated. Flow cytometry analysis (**L**) and corresponding semiquantitative analysis (**M**) of PD-1 in CD8^{+} T cells in tumor tissues after different treatments as indicated. Data in **C–G**, **I–K**, and **M** were represented as the mean ± SD, p values were calculated by one-way ANOVA with Tukey's multiple comparisons, $n = 5$ mice. **N** Schematic illustration of the in vivo study schedule of the CD8^{+} T and NK-cell depletion assay, the figure was created in BioRender. Yujie (2024) https://BioRender.com/g13k834. **O** Tumor growth curves of H22 tumor-bearing mice after different treatments as indicated, (group I and VI ($n = 8$ mice), group II, III, and IV ($n = 10$ mice)). Data in **C** was presented as the mean ± SEM, p value was calculated by two-way ANOVA with Tukey's multiple comparisons. Bac bacteria, MWA microwave ablation. Source data are provided as a Source Data file.

significant contribution of these two cell subsets in facilitating the therapeutic efficacy of 15&15R@VNP synergistic MWA therapy.

The initiation of antigen-specific CD8^{+} T cell responses critically depend on the assistance of mature DCs. While MWA alone may provide a partial tumor antigen pool, it lacks the capacity to stimulate DCs maturation without appropriate adjuvants. VNP20009, despite its modified lipopolysaccharide (LPS) that avoids TLR4 receptor activation, retains the ability to activate TLR5 receptors[41]. TLR5 is a pattern recognition receptor that recognizes flagellin and activates DCs[42,43]. The enhancement of CD8^{+} T cell and NK cell function in the TME is dependent on their adequate presence. Previous study has revealed that the administration of VNP20009 during tumor treatment is accompanied by an elevation in CXCL10 levels[44]. Notably, CXCL10 is a chemokine with the capacity to recruit activated CD8^{+} T cells and NK cells by binding to their receptor, CXCR3[45]. Consistently, our assessment of intratumoral CXCL10 levels revealed an upward trend in the presence of bacteria, compared to the control group (Supplementary Fig. 19). Additionally, we performed in vitro stimulation of DCs maturation using heat-inactivated bacteria. The results demonstrated that both the engineered bacteria prior to and following induction were capable of stimulating DCs maturation comparable to that induced by LPS. Furthermore, these mature DCs secreted substantial quantities of TNF-α, IL-6, and CXCL10 (Supplementary Fig. 20). Collectively, these findings demonstrate that 15&15R@VNP amplifies the effectiveness of MWA therapy by enhancing the functionality of CD8^{+} T cells and NK cells. Considering the important role of CD8^{+} T cells in triggering tumor-specific adaptive immunity, further optimizing the functional role of CD8^{+} T cells is imperative for achieving superior treatment outcomes.

ICB antibody therapy reinvigorates Tpex and further boosts the therapeutic efficacy of 15&15R@VNP in assisting MWA

The mechanistic investigations highlighted the crucial role of CD8^{+} T cells in driving therapeutic efficacy and revealed an exhaustion state characterized by upregulated PD-1 expression on CD8^{+} T cells within the TME. Based on these findings, our next objective is to utilize ICB therapy to reinvigorate dysfunctional T-cell responses by targeting the PD-1/PD-L1 axis. However, exhausted CD8^{+} T cells within the TME often exhibit phenotypic and functional heterogeneity. One distinct subset of exhausted CD8^{+} T cells, referred to as "progenitor" or "stem-like" cells (Tpex), can be identified by intermediate expression of PD-1 and the transcription factor T cell factor 1 (Tcf1, encoded by Tcf7)[46]. In contrast, terminally exhausted T cells (Tex) express high levels of PD-1, T cell immunoglobulin mucin-containing molecule 3 (Tim-3), and other co-inhibitory receptors[47]. It is worth noting that Tpex cells are the only subset of cytotoxic T lymphocytes (CTLs) that responds to PD-1 immune checkpoint inhibitors[48–50]. Interestingly, as anticipated, the combination of MWA therapy with 15&15R@VNP demonstrated a significant enhancement in the expansion of intratumoral Tpex cells compared to the control group and the MWA + VNP20009 group (Fig. 6A). Additionally, previous studies have demonstrated that Tpex cells also express CXCR3[47], enabling them to respond to the elevated

CXCL10 levels and be recruited within the TME. Similarly, the expression of CXCR3 was predominantly observed in most CD8^{+} T cells within tumor tissues of mice treated with MWA + 15&15R@VNP, in comparison to the control group and the MWA + VNP group (Fig. 6B, C).

To investigate the role of IL-15&IL-15Rα in promoting immune cell functions, we performed transcriptome sequencing analysis of the lymphocytes from treated tumor tissues. This method identified 2995 differentially expressed genes, with 1131 transcripts upregulated and 1864 transcripts downregulated in tumor tissue-derived lymphocytes of MWA + IL-15&IL-15R@VNP treated mice compared with those from the control mice (Fig. 6D). Gene Ontology (GO) enrichment analysis showed that the upregulated genes were enriched in several immune-related pathways, including antigen binding, innate immune responses, adaptive immune responses, cytokine mediated signaling pathways, and positive regulation of NF-κB transcription factor activity, etc. (Fig. 6E). These upregulated transcripts in MWA + IL-15&IL-15R@VNP treated mice further indicate that our engineered bacteria in assisting MWA therapy could potently enhance immune responses. Subsequent sequencing also proved that genes involved in the pathways associated with IL-15&IL-15R-mediated T cell activation, specifically the RAS, NF-κB, MAPK, and JAK-STAT pathways, exhibited upregulation (Fig. 6F). Most importantly, the expression of proliferation-related factor (Mki67), anti-apoptosis-related protein (Bcl2) and functional cytokines (Prf1, Grzb, IFN-γ) were also increased (Supplementary Fig. 21A–F). Subsequently, to further verify the mechanism, we sorted tumor-derived CD8^{+} T cells and stimulated with IL-15&IL-15Rα (Fig. 6G). The results showed that compared with IL-2, CD8^{+} T cells treated with IL-15&IL-15Rα were mostly in the precursor exhaustion stage rather than the terminal exhaustion (Fig. 6H and Supplementary Fig. 22). It was further found that after the IL-15&IL-15Rα treatment, more PD-1^{+}CD8^{+} T cells expressed Ki-67, a cell-proliferation marker, demonstrating that IL-15&IL-15R promotes the proliferation of PD-1^{+}CD8^{+} T cells (Supplementary Fig. 23). These Tpex cells, when the PD-1-PD-L1 axis is blocked, can effectively play their tumor killing function. These data provide strong evidence for the implementation of ICB therapy. Collectively, we propose that the sustained activity of CXCR3^{+}CD8^{+} T cells, particularly Tpex cells may be attributed to IL-15&IL-15Rα produced by 15&15R@VNP upon MWA treatment.

Motivated by the promising results mentioned above, a concurrent study was initiated to systematically investigate the anti-tumor effects elicited by reinvigorated Tpex cells. As shown in Fig. 6I, CT26 tumor-bearing mice were randomly divided into 5 groups and subjected to the following treatments once the tumor volume reached approximately 100 mm³: group I received PBS administration (control), group II received MWA treatment alone (MWA), group III received combined MWA and anti-PD-1 treatment (MWA + anti-PD-1), group IV received combined MWA and 15&15R@VNP treatment (MWA + 15&15R@VNP), and group V received combined MWA and 15&15R@VNP treatment, with administration of anti-PD-1 (MWA + 15&15R@VNP + anti-PD-1). The engineered bacteria were intravenously injected into the mice with a dosage of 2×10^6 CFU per mouse on day 0. MWA treatment was carried out for tumors in groups II, III, IV, and V on
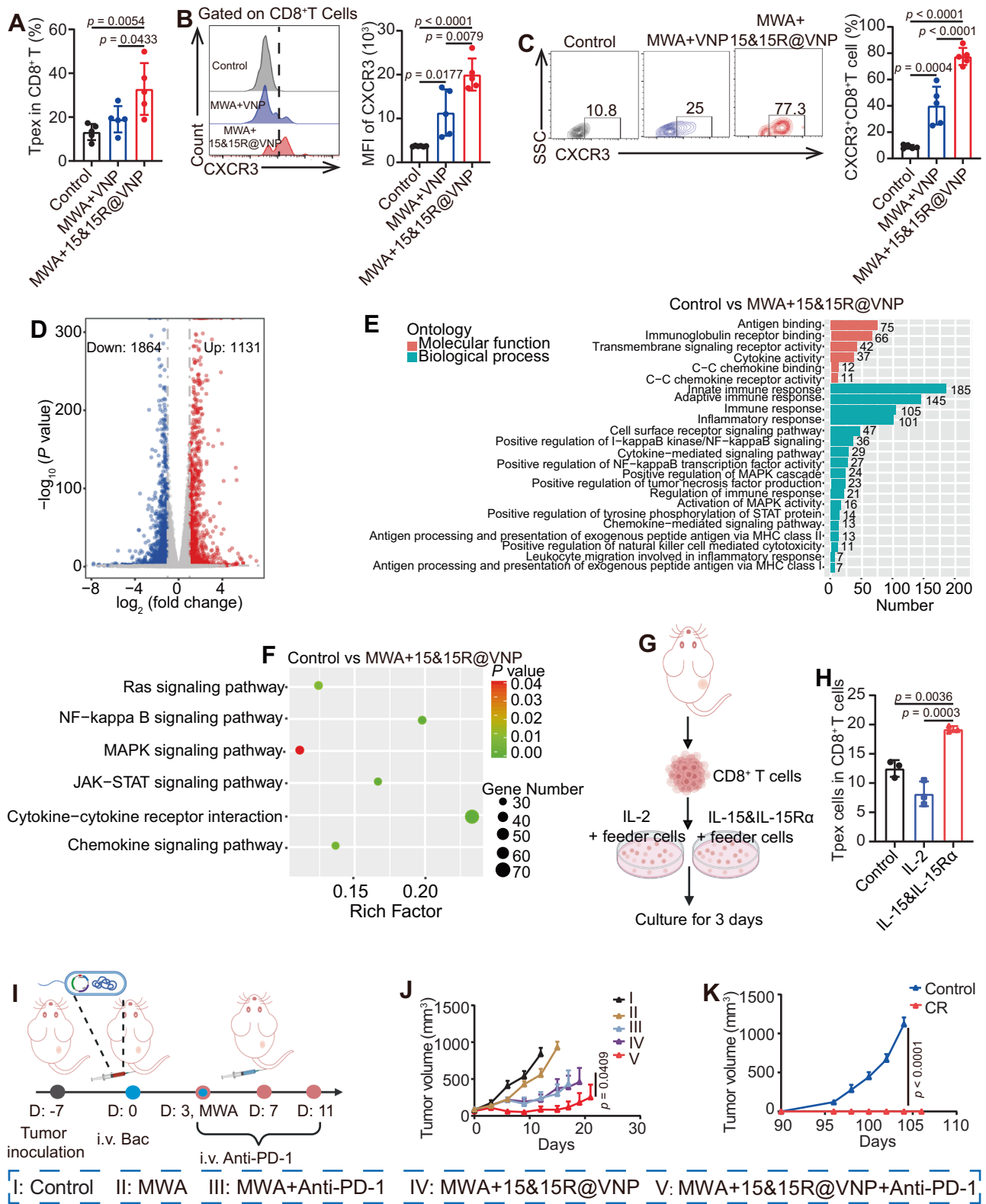
day 3. Anti-PD-1 was administered intravenously on days 3, 7, and 11 at a dose of 20 μg per injection. As anticipated, the concomitant administration of anti-PD-1 noticeably augmented the therapeutic efficacy of 15&15R@VNP-assisted MWA therapy (Fig. 6J and Supplementary Fig. 24). This enhancement was evident not only in the suppression of tumor growth, but also in the prolonged survival of tumor-bearing mice with a notable CR rate of five out of eight (Supplementary Fig. 25). At the 90-day time point, we performed an immunological memory

analysis on the peripheral blood of these cured mice. As expected, a significant increase in the proportion of effector memory T cells (T_{em}) was observed in the peripheral blood circulation of the cured mice, as compared to the control mice (Supplementary Fig. 26). Subsequently, a rechallenge experiment was conducted on cured mice, where equivalent numbers of CT26 tumor cells were inoculated to both cured and age-matched control mice on day 90. Notably, the cured mice displayed no tumor growth, indicating the establishment of long-

Fig. 6 | ICB antibody therapy to boost 15&15R@VNP-assisted MWA tumor treatment. A Intratumoral percentages of Tpex cells (CD3$^+$CD8$^+$PD-1$^+$TCF1$^+$) after different treatments as indicated. **B** Flow cytometry analysis (left) and corresponding semiquantitative analysis (right) of CXCR3 in CD8$^+$ T cells in tumor tissues after different treatments as indicated. **C** Flow cytometric analysis (left) and proportions (right) of CXCR3$^+$CD8$^+$ T cells (CD3$^+$CD8$^+$CXCR3$^+$) in tumor tissues after different treatments as indicated. Data in **A**–**C** were presented as the mean ± SD. *p* values in were calculated by one-way ANOVA with Tukey's multiple comparisons, *n* = 5 mice. **D** On day 3 after treatment, control and MWA + 15&15R@VNP-treated tumor tissues derived lymphocytes were taken for transcriptome sequencing. The overall distribution of regulated genes is represented by a volcano plot, in which the abscissa and ordinate represent the fold change of gene expression in different samples and statistical significance (*p* value) of the difference in gene expression, respectively. The red, blue and gray dots represent the upregulated, downregulated and no significant changes of genes, respectively. Statistical significance was calculated via two-tailed Student's *t* test (*n* = 3 samples). **E** GO enrichment analysis of the upregulated genes in tumor tissues-derived lymphocytes from the MWA + 15&15R@VNP-treated mice. **F** The enrichment scatter plot to show KEGG enrichment analysis of a selection of immune-related KEGG terms. Statistical significance was calculated via two-tailed Student's *t* test (*n* = 3 samples). **G** Schematic illustration of the sorting and treatment of tumor-derived CD8$^+$ T cells in tumor-bearing mice, the figure was created in BioRender. Yujie (2024) https://BioRender.com/o71q099. **H** The percentage of Tpex cells under different treatments, data in **H** was presented as the mean ± SD, *p* values were calculated by one-way ANOVA with Tukey's multiple comparisons, *n* = 3 samples. **I** Schematic illustration of the in vivo treatment schedule by combining ICB therapy with 15&15R@VNP-assisted MWA for CT26 tumor model, the figure was created in BioRender. Yujie (2024) https://BioRender.com/g13k834. **J** Tumor growth curves of CT26 tumor-bearing mice after different treatments as indicated (group I, II, and IV (*n* = 6 mice), group III and V (*n* = 7 mice)). **K** Tumor growth curves of tumor rechallenge experiment in CT26 tumor-bearing mice as indicated (*n* = 5 mice). Data in **J** and **K** were presented as the mean ± SEM and the *p* values were calculated by two-way ANOVA with Tukey's multiple comparisons. Bac bacteria, MWA microwave ablation. Source data are provided as a Source Data file.

lasting immune memory against the primary tumor and potential protection against recurrence (Fig. 6K).

Augmented tumor regression via in situ stimulation of Tpex cells using engineered sPD-1-15&15R@VNP

Inspired by the ability of anti-PD-1 ICB therapy to boost the therapeutic efficacy of 15&15R@VNP-assisted MWA treatment, we designed a innovative type of engineered bacteria to co-express IL-15&IL-15Rα and sPD-1 (Fig. 7A). The successful construction of sPD-1@VNP and sPD-1-15&15R@VNP vectors was confirmed through restriction enzyme digestion and DNA gel electrophoresis (Supplementary Fig. 27). Similarly, protein expression was confirmed in the engineered bacterial strains, with sPD-1 expressed in sPD-1@VNP and both sPD-1 and IL-15&IL-15Rα expressed in sPD-1-15&15R@VNP, upon being induced at a temperature around 42–47 °C (Supplementary Fig. 28). Next, we performed in vivo experiments in CT26 tumor-bearing mice. Once the tumor volume reached approximately 100 mm^3, the mice were randomly divided into five groups and subjected to the following treatments: group I received PBS administration (control), group II received MWA treatment alone (MWA), group III received combined MWA and sPD-1@VNP treatment (MWA + sPD-1@VNP), group IV received combined MWA and 15&15R@VNP treatment (MWA + 15&15R@VNP), and group V received combined MWA and sPD-1-15&15R@VNP treatment (MWA + sPD-1-15&15R@VNP). After 3 days, MWA treatment was carried out for tumors in groups II, III, IV, and V. By monitoring the tumor growth, we found that the engineered bacteria that simultaneously express IL-15&IL-15Rα and sPD-1 exhibited remarkable therapeutic efficacy when combined with MWA (group V), compared with other groups (Fig. 7B). Moreover, this therapeutic approach realized significant inhibition of tumor growth and a noticeably prolonged survival rate, with a CR rate of six out of eight (Fig. 7C and Supplementary Fig. 29). PD-L1 expression was positive in tumors of all groups as indicated by immunohistochemistry (IHC) staining (Fig. 7D). However, TUNEL and H&E staining of tumor tissue sections further evidenced the profound therapeutic effect achieved by MWA assisted by sPD-1-15&15R@VNP (Fig. 7E, F).

Previous studies have confirmed that PD-L1 or PD-1 blockade promotes the expansion and differentiation of Tpex cells into highly cytolytic transient exhausted CD8$^+$ T cells, characterized by their strong cytolytic activity and co-expression of GzmB[50,51]. These cells would further progress into terminally exhausted CD8$^+$ T cells, which exhibit functional impairment. Seeking to validate the functionality of Tpex cells further reinvigorated by the MWA combined with sPD-1-15&15R@VNP therapy, a set of immune evaluation models consistent with previous treatment was initiated. On the third day post-MWA

treatment, mice from each experimental group were euthanized, with their tumors collected for subsequent analysis. Our results demonstrated that, compared to the MWA group (group II), mice treated with MWA combined with the 15&15R@VNP group (group IV) showed increased Tpex cells in TME. Furthermore, mice treated with MWA combined with sPD-1-15&15R@VNP (group V) exhibited a more pronounced enhancement of Tpex cells as a result of the interference with the PD-1/PD-L1 axis (Fig. 7G and Supplementary Fig. 30). Moreover, this combined treatment (group V) significantly enhanced Tpex cell proliferation, as indicated by a pronounced upregulation of Ki67 expression, compared to that in group III (Fig. 7H and Supplementary Fig. 30). Our results suggest that the combination of MWA with sPD-1-15&15R@VNP therapy contributes to the enrichment of the "Tpex cell pool". A more noteworthy observation is that, compared to MWA + 15&15R@VNP (group IV), there was a discernible upregulation in the proportion of Tex cells for mice treated with MWA + sPD-1-15&15R@VNP (group V) (Fig. 7I). This observation indicated that the disruption of the PD-1/PD-L1 axis by sPD-1 would further enhance the differentiation of Tpex cells towards terminal exhaustion, facilitating the residual functionality of Tpex cells. This hypothesis was further supported by the subsequent upregulation of Grzb$^+$PD-1$^+$CD8$^+$ T cells (Fig. 7J and Supplementary Fig. 30), underscoring the unleashed functionality of Tpex cells following the blockade of PD-1/PD-L1 axis.

Previous studies have demonstrated that antigen-specific CD8$^+$ T cells are initially activated by tumor antigen stimulation within the TDLNs during tumor initiation and progression. These cells would undergo differentiation into Tpex and subsequently migrate into the TME, where they would extensively differentiate into Tex[52]. To assess the role of Tpex, we employed the S1PR1 inhibitor FTY720 to impede the migration of newly activated T cells, including Tpex, from lymphoid organs into the tumor tissue[53]. As illustrated in Fig. 7K, CT26 tumor cells were inoculated 7 days before the experiment. On day 0, engineered bacteria were intravenously injected at a dose of 2×10^6. FTY720 was administered intravenously on day 2 (1 day prior to the MWA treatment) and continued every other day at a dose of 20 µg per mouse. MWA was conducted on day 3. By monitoring the tumor growth, we found that FTY720 largely attenuated the therapeutic efficacy of sPD-1-15&15R@VNP-assisted MWA treatment (Fig. 7L). As Tpex is the only type of immune cells that truly respond to ICB therapy, our results indicate that Tpex plays a pivotal role in the efficacy of MWA combined with sPD-1-15&15R@VNP treatment. Therefore, our findings demonstrate that sPD-1-15&15R@VNP combined with MWA could effectively improve Tpex cell functionality, resulting in superior tumor-suppression efficacy without the need of additional ICB antibodies.
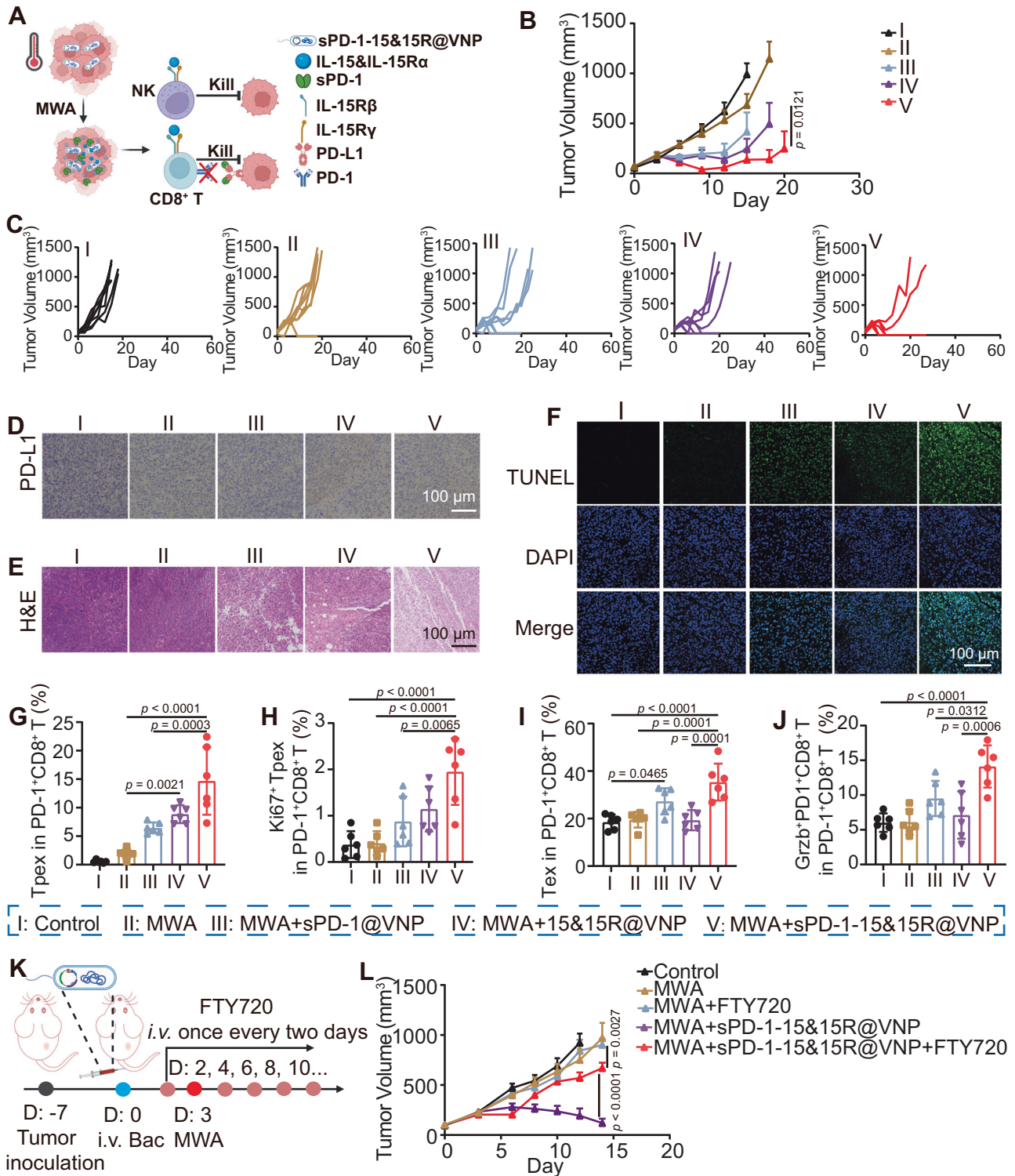
Fig. 7 | Enhanced tumor regression by in situ promotion of Tpex cells through engineered sPD-1-15&15R@VNP. A Schematic illustration of the mechanism by which engineered bacteria achieve simultaneous intratumoral ICB and sustained activation of immune cells under MWA initiation, the figure was created in BioRender. Yujie (2024) https://BioRender.com/b85q249. Tumor growth curves (**B**, group I and IV (*n* = 7 mice), group II, III, and V (*n* = 8 mice)), individual tumor growth curves (**C**), magnified PD-L1 staining images (**D**), magnified H&E staining images (**E**), and magnified TUNEL staining images (**F**) of tumor sections of CT26 tumor-bearing mice after different treatments as indicated. Data in **B** was presented as the mean ± SEM, *p* value was calculated by two-way ANOVA with Tukey's multiple comparisons. Intratumoral percentages of Tpex cells (**G**, CD3+CD8+PD-1+TCF1+), Ki67+ Tpex cells (**H**, CD3+CD8+PD-1+TCF1+Ki67+), Tex cells (**I**, CD3+CD8+PD-1+TCF1−)

and Grzb+PD-1+ T cells (**J**, CD3+CD8+PD-1+Grzb+) after different treatments as indicated (*n* = 6 mice). Data in **G**–**J** were presented as the mean ± SD, *p* values were calculated by one-way ANOVA with Tukey's multiple comparisons. **K** Schematic illustration of the experiment design by using FTY720 to inhibit lymphocyte migration, the figure was created in BioRender. Yujie (2024) https://BioRender.com/r47l430. **L** Tumor growth curves of CT26 tumor-bearing mice after different treatments as indicated (group I, III, and IV (*n* = 7 mice), group II and V (*n* = 6 mice)). Data in **L** was presented as the mean ± SEM, *p* values were calculated by two-way ANOVA with Tukey's multiple comparisons. MWA microwave ablation, Bac bacteria. Source data are provided as a Source Data file.

sPD-1-15&15R@VNPs boost the efficacy of MWA in the treatment of in situ liver cancer and the long-term safety of this therapy

To further emulate clinical MWA for liver cancer, we constructed engineered bacteria RsPD-1-15&15R@VNP secreting rat IL-15&IL-15Ra and sPD-1 proteins. The engineered RsPD-1-15&15R@VNP could efficiently secrete rat IL-15&IL-15Ra and sPD-1 proteins under MWA (Supplementary Fig. 31). Next, the antitumor efficacy of RsPD-1-15&15R@VNP boosted MWA treatment was further confirmed in a highly malignant orthotropic N1S1 HCC rat tumor model. Briefly, 14 SD rats bearing N1S1 orthotopic tumors (~100 mm³) were divided into three groups and treated as below: group I, Control ($n = 4$); group II, MWA ($n = 5$); group III, MWA + RsPD-1-15&15R@VNP ($n = 5$). These SD rats of group III were intravenously injected with RsPD-1-15&15R@VNP at day 0 at a dose of 2×10^7 CFU (200 µL), while these SD rats of groups II and III were subjected to MWA treatment at day 3. At day 0 before different treatments and 7, 14 days post different treatment, these rats were then subjected to a 3.0-T MRI imaging system for recording the tumor volumes (Fig. 8A). During MWA, the temperature of the tumor site was continuously monitored using an infrared thermometer, ensuring that it remained around 42–47 °C (Fig. 8B, C). We found that engineered RsPD-1-15&15R@VNP combined with MWA showed highly effective tumor inhibitory effect, with all 5 of 5 rats cured at 14 days post corresponding treatment, much more effective than MWA alone (Fig. 8D–H).

As accumulating reports have demonstrated that ICB therapy would cause potential systemic inflammation or autoimmunity concern[54], we then carefully evaluated the potential toxic effects our proposed cancer treatment strategy in a long-term experimental model. We treated 15 mice bearing H22 tumors according to the previous treatment regimen (Fig. 8I). The seven cured mice were sacrificed for hematologic and histopathology alterations after 1 months. Notably, we observed no changes in red blood cells (RBC), total hemoglobin (Hb), blood hematocrit (HCT), platelets (PLT), hemoglobin (HGB), mean corpuscular volume (MCV), mean corpuscular hemoglobin (MCH), and mean corpuscular hemoglobin concentration (MCHC), as well as slightly decreased hematocrit (HCT), and mean corpuscular volume (MCV) among the majority of the mice treated with MWA + sPD-1-15&15R@VNP (Fig. 8J–L). The presentation of leukocytes was largely normal (Supplementary Fig. 32). These data demonstrate that the combination of MWA and engineered sPD-1-15&15R@VNP did not cause significant hemolysis or inflammation. After necropsy, it is clear that erythrocyte production in the bone marrow was also not severely restricted, and the bone and bone marrow of MWA + sPD-1-15&15R@VNP treated mice were comparable to those of control mice (Fig. 8M). To quantitate the defects in the red cell lineage in the bone marrow, we analyzed the distribution of CD71 and Ter119 markers among the bone marrow cells as well as the cell sizes. These markers have been used to mark five stages of erythrocyte development: stage I, CD71⁺Ter119⁻; stage II, FSC-A^hi CD71⁺Ter119⁺; stage III, FSC-AmiCD71⁺Ter119⁺; stage IV, FSC-A^lo CD71⁺Ter119⁺; and stage V, CD71⁻Ter119⁺. As shown in Fig. 8N, O, MWA + sPD-1-15&15R@VNP treated mice exhibited similar distribution and maturation states of erythrocytes in the bone marrow compared with control mice. Taken together, our results demonstrated that sPD-1-15&15R@VNP boosted MWA treatment could induce effective tumor suppression without imposing obvious side effects.

Discussion

Improving response rates and reducing side effects remains a major challenge for cytokine-based cancer immunotherapy[55]. Despite various modifications aiming at increasing the tumor-targeting specificity of cytokines and reducing immune-related adverse events (irAEs), the results have not been entirely satisfactory[56]. In this work, we have shown that through genetic engineering of attenuated *Salmonella typhimurium* strain VNP20009, we can induce the secretion of

therapeutic cytokines upon external thermal induction. By harnessing the tumor-restricted growth of VNP20009, we can effectively trigger the production of cytokines and other therapeutic proteins directly within the tumor post MWA treatment. Specifically, we observed that the tumor-localized expression of IL-15&IL-15Rα by 15&15R@VNP could be turned-on by MWA treatment, with minimal upregulation of IL-15&IL-15Rα and other pro-inflammatory cytokines in the peripheral blood of tumor-bearing mice. As the results, intravenous administration of 15&15R@VNP could great boost the antitumor immunity post incomplete MWA treatment as evidenced by suppressed tumor growth and prolonged animal survival, owing to the ability of continuously produced IL-15&IL-15Rα in situ to sustain the activities of CD8⁺ T cells and NK cells.

Considering the exhaustion of activated CD8⁺ T cells that occurs following prolonged antigen exposure as indicated by the upregulation of Tpex cells, we further found that ICB antibodies could be used to enhance the tumor suppression efficacy of 15&15R@VNP-assisted MWA treatment, by blocking the PD-1/PD-L1 axis and reinvigorating Tpex cells. Inspired by this finding, we thus designed the advanced version of engineered bacteria that could produce sPD-1 together with IL-15&IL-15Rα under thermal induction. Interestingly, such sPD-1-15&15R@VNP exhibited a prominent synergistic effect when combined with MWA, leading to further improved inhibition of tumor growth by fully reinvigorating the anti-tumor effects of Tpex cells. Additionally, in the orthotopic liver cancer model, rats treated with MWA combined with RsPD-1-15&15R@VNP demonstrated a potent antitumor effect. Moreover, safety evaluations suggested a negligible risk of irAE and indicated favorable biosafety. Considering it needs some time for IL-15&IL-15Rα to promote T cell proliferation, in the further study, sequential expressing system can be designed to optimize the therapeutic outcomes.

In conclusion, our study demonstrates that engineered bacteria can be activated by MWA to secret cytokines within the tumor, effectively maintaining immune cell activity and reversing exhaustion, thereby attenuating tumor growth and significantly prolonging the survival of tumor-bearing mice. This system offers a valuable opportunity to connect the modulation of the TME with localized ICB through the use of engineered bacteria as live drugs. Importantly, our system can effectively reinvigorate Tpex cells, the major subset of cells responsive to ICB therapy. Given that our system has the potential to effectively expand the "Tpex cell pool", it serves as an excellent alternative therapy, especially for individuals with a poor response to ICB. Our treatment procedure allows for the seamless integration of hyperthermia, immune response amplification, and ICB, thereby establishing a comprehensive three-pronged strategy for combating tumors.

Methods

Ethics approval

The animal procedures were performed with ethical compliance and approval by the Institutional Animal Care and Use Committee at Soochow University with an approval number of SYXK(Su)2021-0073. All the animal experiments were conducted in compliance with the Regulations for the Administration of Affairs Concerning Experimental Animals of China. All the animal experiments complied with institutional guidelines.

Materials

Anti-mouse PD-1 monoclonal antibody (cat. no. BE0273) was obtained from BioXcell (New Hampshire, USA). Anti-mouse CD8α monoclonal antibody (cat. no. 100763), anti-mouse Asialo GM1 monoclonal antibody (cat. no. 146002), anti-mouse CD45-Percp (cat. no. 1009825), anti-mouse CD11c-FITC (cat. no. 117305), anti-mouse CD80-APC (cat. no. 104713), anti-mouse CD86-PE (cat. no. 105007), anti-mouse CD3-FITC (cat. no. 100203), anti-mouse CD4-APC (cat. no. 100411), anti-
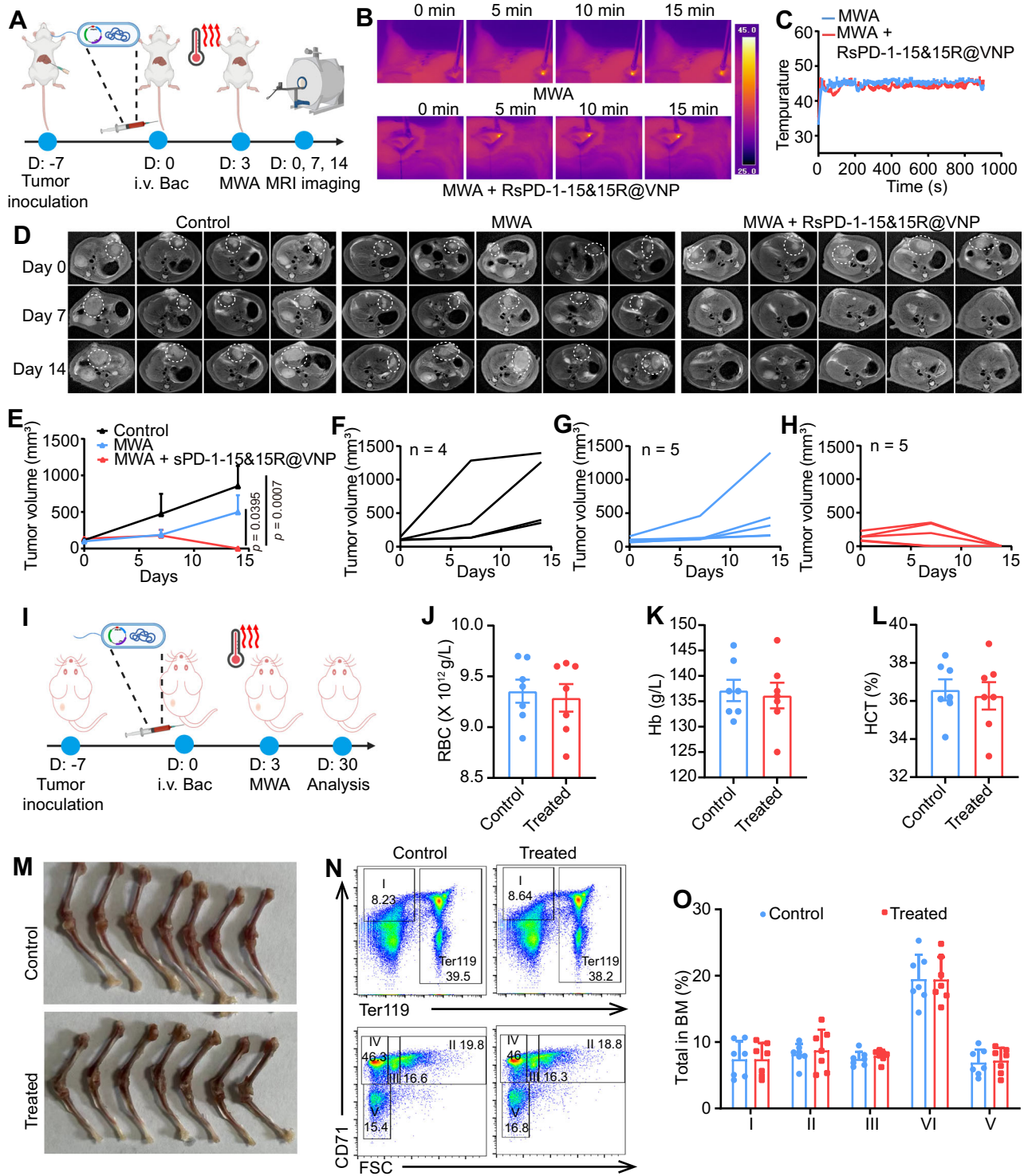
Fig. 8 | sPD-1-15&15R@VNP boosted the efficacy of MWA in the treatment of in situ liver cancer and the long-term safety of this therapy. A Schematic illustration of in vivo therapeutic schedule in N1S1 rat tumor model, this figure was created in BioRender. Yujie (2024) https://BioRender.com/o1lo903. Representative thermal images (**B**), and corresponding microwave heating profiles (**C**) of mice after different treatments as indicated (*n* = 3 rats). Corresponding T1 contrast-enhanced MRI scanning of N1S1 bearing rats with different treatments as indicated tumor curves (**D**), average (**E**, control (*n* = 4 mice), the other two groups (*n* = 5 mice)) and individual (**F**–**H**) tumor growth curves of different groups of N1S1 bearing rats after various treatments as indicated. Data in **E** was presented as the mean ± SEM and the *p* values were calculated by the two-way ANOVA with Tukey's multiple comparisons. **I** Schematic illustration of in vivo evaluation of irAE risk of engineered sPD-1-

15&15R@VNP combined with MWA in H22 mouse tumor model, this figure was created in BioRender. Yujie (2024) https://BioRender.com/i42a859. The measured parameters included red blood cells (RBC, **J**), hemoglobin (Hb, **K**), and hematocrit (HCT, **L**) collected from these mice at day 30. **M** Generation of red cells in bone marrow. Representative FACS profiles (**N**) and analysis (**O**) of depicting distribution of Ter119, CD71 and forward scatters (FSC-A) among bone marrow cells. The gating and % of cells at stage I–V are indicated. Data in **J**–**L**, and **O** were presented as the mean ± SD and the *p* values were calculated by the two-tailed Student's *t* test (**J**–**L**) and two-way ANOVA with Tukey's multiple comparisons (**O**), *n* = 7 mice. Bac bacteria, MWA microwave ablation. Source data are provided as a Source Data file.

mouse CD8α-PE (cat. no. 100707), anti-mouse CD45-FITC (cat. no. 157608), anti-mouse CD3-APC (cat. no. 100235), anti-mouse CD49b-Percp-cy5.5 (cat. no. 103519), anti-mouse Ki67-FITC (cat. no. 652409), anti-mouse CD69-FITC (cat. no. 104506), anti-mouse IFN-γ-PE (cat. no. 163504), anti-mouse PD-1-APC (cat. no. 109112), anti-mouse CXCR3-PE-cy7 (cat. no. 126515), and anti-mouse Grzb-PE-cy7 (cat. no. 372213) were purchased from BioLegend (San Diego, USA). Anti-mouse CD44-PE (cat. no. 12-0041), anti-mouse CD62L-APC, and anti-mouse CD8α- Percp-cy5.5 (cat. no. 45-0081), and anti-mouse TCF1-Alexa Flour 594 (cat. no. FAB8224T-100UG) were obtained from Invitrogen (Carlsbad, USA). Mouse cytokine ELISA kits for IFN-γ, and IL-15&IL-15Rα were ordered from Invitrogen (Carlsbad, USA). Lysogeny broth (LB) was purchased from Beijing Land Bridge Technology Co., Ltd. (China).

Bacteria strain and plasmids

Attenuated *Salmonella typhimurium* (VNP20009) used in this study was obtained from the School of Radiation Medicine and Protection at Soochow University and has been maintained in our laboratory. To generate IL-15&IL-15Rα-expressing VNP20009, the pBV-15&15Ra plasmid was constructed by inserting the soluble region (amino acids 1-173) of IL-15 (UniProt accession number P48346) and IL-15Rα (UniProt accession number Q60819) with a His-Tag into the pBV220 plasmid using the multiple cloning site. The IL-15 and IL-15Ra were linked with a flexible linker. to facilitate the secretion of IL-15&IL-15Rα, a pelb signal peptide sequence was introduced at the N-terminus of the fusion protein. Next, the pBV-15&15Rα plasmid was transformed into VNP20009 using a heat shock transformation method, yielding engineered bacteria strains named as 15&15R@VNP. To prepare VNP20009 expressing soluble PD-1 (sPD-1), the pBV-sPD-1 plasmid was constructed by inserting the soluble region of the PD-1 sequence (UniProt accession number Q02242) with a pelB signal peptide sequence at the N-terminus, into the pBV220 plasmid at the multiple cloning site. Subsequently, the pBV-sPD-1 plasmid was transformed into VNP20009 using a similar method, yielding engineered bacteria strains named as sPD-1@VNP. To prepare VNP20009 co-expressing sPD-1 and IL-15&IL-15Rα, the pBV-sPD-1-IL-15&IL-15Rα plasmid was created by cloning both sPD-1 and IL-15&IL-15Rα sequences into the pBV220 plasmid. These plasmids were then similarly transformed into VNP20009, yielding engineered bacteria strains named as sPD-1-15&15R@VNP. To prepare VNP20009 expressing mCherry, the pBV-mCherry plasmid was constructed by inserting the mCherry sequence into the pBV plasmid at the multiple cloning site and transformed into VNP20009 using a similar method, yielding engineered bacteria strains named as mCherry@VNP. To prepare VNP20009 co-expressing Rat sPD-1 and Rat IL-15&IL-15Rα, both of the exogenous genes in pBV-sPD-1-IL-15&IL-15Rα plasmid were replaced with those of rats, and transformed into VNP20009 using a similar method, yielding engineered bacteria strains named as RsPD-1-15&15R@VNP. All acquired strains were cultured in LB medium containing 100 μg ml^{-1} ampicillin and stored as 25% glycerol stocks at −80 °C until further use.

Characterization of constructed strains

To verify the protein expression of engineered bacteria strains, VNP20009 strains with different modifications were incubated in an LB medium supplemented with ampicillin (100 μg ml^{-1}). The bacteria cultures were grown in an oscillating incubator until the optical density (OD$_{600}$) reached 0.4 to 0.6 at 37 °C. Subsequently, the cultures were induced at 42 °C for varying durations and then returned to 37 °C for an additional 6 h of incubation. The protein expression of mCherry was detected by the IVIS system. Meanwhile, to validate the protein expression of sPD-1@VNP, 15&15R@VNP, sPD-1-15&15R@VNP, and RsPD-1-15&15R@VNP, the bacteria cell pellets and supernatants were collected. SDS-PAGE and western blot analysis were performed to detect the expression of the respective proteins in the cell pellets and supernatants. All unprocessed western blot images have been shown in Supplementary Fig. 33.

Animals and cells

Female BALB/c mice (6–8 weeks) and Sprague-Dawley (SD) rats were procured from the Laboratory Animal Center of Soochow University and utilized by the approved protocols of the Laboratory Animal Center of Soochow University.

H22 cells and CT26 cells were purchased from Cell Bank, Shanghai Institutes for Biological Sciences, Chinese Academy of Sciences were cultured in Roswell Park Memorial Institute 1640 media (HyClone) containing 10% fetal bovine serum (Gibco) and 1% PS at 37 °C in 5% CO$_2$. Rat N1S1 hepatocellular carcinoma cell was obtained from Lishui Hospital of Zhejiang University as a gift, and maintained with DMEM high-glucose medium supplemented with 10% FBS and 1% penicillin/streptomycin.

Cellular experiments

For T cell isolation, Balb/c mice aged 8–10 weeks were sacrificed for cervical dislocation. The spleen was obtained, and gently ground with the piston of a 5 ml syringe, then the tissue was filtered with a 40 micrometers filter membrane. The white blood cells of the spleen were obtained by lysis of red blood cell lysate for 5 min. CD3 antibody labeled with magnetic beads (Biolegend, USA) was incubated with these spleen leukocytes at 37 °C for 30 min, centrifuged at 4 °C, 500 × g for 5 min, and then the free magnetic beads were washed away. Then CD3$^+$ T cells were sorted by magnetic rack. These sorting cells were cultures with 1640 complete medium containing 5 μg ml^{-1} anti-CD3, 10 μg ml^{-1} anti-CD28 and 10 ng ml^{-1} IL-2 for 72 h.

To validate the activity maintenance of IL-15&IL-15Rα protein expressed by 15&15R@VNP on T cells, we purified the expressed fusion protein using a nickel chelated column (GenScript, Nanjing, China) according to the according to the manufacturer's instructions, and the concentration of the purified IL-15&IL-15Rα was measured with BCA protein assay kit (Thermo Scientific, USA). CFSE-labeled T cells were then stimulated with IL-15&IL-15Rα protein at a concentration of 20 ng mL^{-1}. After 72 h, T cell proliferation was assessed by flow cytometry.

Tumor model

Subcutaneous H22 tumor models and CT26 tumor models were developed by subcutaneously injecting H22 tumor cells (2×10^6) and CT26 cells (2×10^6) into the right inguinal region of each mouse, respectively. To establish an orthotopic N1S1 tumor model, N1S1 cells (6×10^6) were suspended in 75 μL of PBS containing 30% Matrigel (Corning) and intracapsularly injected into the right lower lobe of the liver in each SD rat under anesthesia, using a 25-gauge syringe needle. For the maximal tumor size/burden, tumor growth was measured by recording tumor length (L) and width (W) using a digital caliper, and tumor volume (V) was calculated as $V = L \times W^2/2$. Mice were euthanized when the tumor size exceeded 1500 mm^3.

Bacterial tumor-specific colonization and biodistribution in vivo

To determine the tumor-targeting ability of the engineered bacteria, healthy or H22-tumor-bearing mice were intravenously administered with 15&15R@VNP. At specified time intervals, the tumor, heart, liver, spleen, lung, and kidney were collected, weighed, and subsequently homogenized using a tissue dissociator under sterile conditions. The resulting homogenates were then diluted with PBS and plated onto LB agar plates. After 24 h of incubation at 37 °C, the bacteria colonies were counted, and the bacteria concentrations (CFU/g tissue) were calculated based on the colony counts, corresponding dilution factors, and tissue weights.

Protein expression of engineered bacteria in vivo

To assess the ability of MWA to induce the expression of proteins by engineered bacteria, H22-tumor-bearing mice were intravenously administered with mCherry@VNP (2×10^6 CFU per mouse) or 15&15R@VNP (2×10^6 CFU per mouse), respectively. After 72 h, the mice were subjected to MWA treatment. For validation of mCherry fluorescent protein expression, tumor tissues were collected at different time points and homogenized using a tissue dissociator under aseptic conditions. The homogenates were then diluted with PBS and plated on LB agar plates. Following incubation at 37 °C for 24 h, the fluorescence of bacteria colonies was detected using the IVIS system. For the detection of IL-15&IL-15Rα protein expression, tumor tissues, and peripheral blood were collected from the mice at different time points. Tumor tissues were weighed, homogenized with a tissue dissociator under aseptic conditions, and centrifuged at $500 \times g/4$ °C for 5 min to obtain the supernatant. Peripheral blood was centrifuged at $500 \times g/4$ °C for 10 min to obtain the serum. The IL-15&IL-15Rα protein content was determined using an ELISA kit specifically designed for IL-15&IL-15Rα detection.

In vivo 15&15R@VNP-mediated therapy

To assess the efficacy of 15&15R@VNP in augmenting the therapeutic potency of MWA, H22 or CT26 tumor-bearing mice were randomly assigned into 6 groups when their tumors reached a volume of approximately 100 mm³: control (group I), MWA (group II), VNP (group III), 15&15R@VNP (group IV), MWA + VNP (group V), MWA + 15&15R@VNP (group VI). Bacteria were intravenously administered on day 0 (2×10^6 CFU per mouse), followed by MWA on day 3. To perform MWA, the MWA needle was inserted vertically into the tumor. The operating frequency of the microwave irradiator was 2.45 GHz, the tumor surface temperature of the mice during microwave exposure was monitored using a thermal camera (Fotric 225). On day 7, one mouse from each group in the H22-tumor-bearing model was randomly selected, and the tumor was collected for evaluation of the early-stage therapeutic efficacy using H&E staining.

In vivo assessment of immune responses

To evaluate the potency of combined 15&15R@VNP and MWA treatment in modulating the TME, H22 tumor-bearing mice were divided into 6 groups and treated as mentioned above when their tumors reached a volume of approximately 100 mm³. On day 7, all mice were sacrificed, and their tumor tissues and adjacent TDLNs were excised. The tissues were then homogenized and enzymatically digested to obtain single-cell suspensions. Then, the percentages of mature DCs (CD45⁺CD11c⁺CD80⁺CD86⁺) inside the TDLNs and CD3⁺ T cells (CD45⁺CD3⁺), CD8⁺ T cells (CD45⁺CD3⁺CD8⁺), CD4⁺ T cells (CD45⁺CD3⁺CD4⁺), NK cells (CD45⁺CD3⁻CD49b⁺), Ki67⁺CD8⁺ T cells (CD45⁺CD3⁺CD8⁺Ki67⁺), activated CD8⁺ T cells (CD45⁺CD3⁺CD8⁺CD69⁺), activated NK cells (CD45⁺CD3⁻CD49b⁺CD69⁺), effector CD8⁺ T cells (CD45⁺CD3⁺CD8⁺IFN-γ⁺), and exhausted CD8⁺ T cells (CD45⁺CD3⁺CD8⁺PD-1⁺) inside the tumors were subjected to flow cytometry for detailed analysis.

To assess the efficacy of combined 15&15R@VNP and MWA treatment in promoting Tpex cell infiltration, H22 tumor-bearing mice were divided into 3 groups and treated as described above upon reaching a tumor volume of approximately 100 mm³. On day 7, all mice were euthanized, and tumor tissues were excised and enzymatically digested to obtain single-cell suspensions. Then, the percentages of Tpex cells (CD45⁺CD3⁺CD8⁺PD-1⁺TCF7⁺) and CXCR3⁺CD8⁺ T cells (CD45⁺CD3⁺CD8⁺CXCR3⁺) inside the tumors were subjected to flow cytometry for detailed analysis.

To assess the potency of combined sPD-1-15&15R@VNP and MWA therapy in reinvigorating Tpex cells, Balb/c mice with subcutaneous CT26 tumors were randomly divided into five experimental groups and described above. On day 7, all mice were euthanized, and the percentages of Tpex cells (CD3⁺CD8⁺PD-1⁺TCF7⁺), Ki67⁺ Tpex cells (CD3⁺CD8⁺PD-1⁺TCF7⁺Ki67⁺), Tex cells (CD3⁺CD8⁺PD-1⁺TCF1⁻) and Grzb⁺PD-1⁺ cells (CD3⁺CD8⁺PD-1⁺Grzb⁺) inside the tumors were subjected to flow cytometry for detailed analysis.

For intracellular staining, tumor single cell suspensions were stimulated in vitro with a cell-stimulating cocktail for 6 h (Thermo Fisher Scientific, CA, USA) at 37 °C. Cells were then surface-stained, fixed, permeabilized, and stained for cytokine production using the Fixation and Permeabilization Buffer Kit per the manufacturer's recommendations (Thermo Fisher Scientific, CA, USA). For Ki-67, Foxp3 and TCF7 staining, the samples were prepared using eBioscience™ Foxp3/Transcription Factor Staining Buffer Set (Thermo Fisher Scientific, CA, USA) after surfaced markers staining. The FACS data were analyzed with Flowjo10 software (version 7.6.5; Tree Star, Ashland, OR, USA),

To further evaluate the immune responses, tumor tissues derived lymphocytes in the control and MWA + 15&15R@VNP groups were collected for transcriptomic analysis. The RNA samples of lymphocytes derived from tumor tissues were collected in accordance with the TRIzol-based procedure. Subsequently, the total RNAs were subjected to analysis by GENEWIZ (Suzhou, China).

IFN-γ detection

The secretion levels of IFN-γ in the homogenized tumor tissues or blood serum were measured by using ELISA kits according to the manufacturer's instructions.

T-cell and NK-cell depletion experiments

T-cell and NK-cell depletion assays were conducted to validate the underlying mechanism of combined 15&15R@VNP and MWA therapy in cancer treatment. Thirty Balb/c mice bearing subcutaneous H22 tumors were randomly divided into 5 groups and treated with PBS (group I), 15&15R@VNP + MWA (group II), 15&15R@VNP + MWA + anti-CD8α (group III), 15&15R@VNP + MWA + anti-ASIO GM1 (group IV), or 15&15R@VNP + MWA + anti-CD8α + anti-ASIO GM1 (group V). Mice in all groups except group I were intravenously administered with 15&15R@VNP on day 0. Three days later, mice receiving engineered bacteria were subjected to MWA To deplete T or NK cells, mice in group III, group IV, or group V were intravenously injected with anti-CD8α (1 mg kg⁻¹ per mouse) or anti-ASIO GM1 (0.5 mg kg⁻¹ per mouse), or a combination of both, on day 3, 5, and 7. The tumor growth and survival of the mice were recorded by the aforementioned methodology.

Tumor model for 15&15R@VNP-assisted ICB

To assess the efficacy of combined 15&15R@VNP and MWA in synergistic ICB therapy, Balb/c mice bearing subcutaneous CT26 or H22 tumors were randomly assigned to five experimental groups. These groups received the following treatments: PBS (group I), MWA alone (group II), 15&15R@VNP + MWA (group III), MWA + anti-PD-1 (group IV), or 15&15R@VNP + MWA + anti-PD-1 (group V). Mice in groups III and V received a tail vein injection of 15&15R@VNP at a dose of 2×10^6 CFU per mouse on day 0. Three days later, MWA was performed on all groups except Group I. Mice in group III or group V received intravenous injections of anti-PD-1 (1 mg kg⁻¹ per mouse) on days 3, 6, and 9. The tumor growth and survival of mice were recorded by the aforementioned methodology.

Immunological memory responses triggered by our combination therapy

To perform the tumor rechallenge experiment, on the 90th day after successful treatment of CT26 tumor-bearing mice with combined 15&15R@VNP + MWA + anti-PD-1 (group V), peripheral blood samples were collected from the cured mice and their paired normal control mice for analysis of the proportion of T_{em} cells

(CD3⁺CD8⁺CD62⁻CD44⁺) in the peripheral blood. Subsequently, subcutaneous inoculation of CT26 tumor cells (2×10^6) was performed. The tumor growth and survival of mice were recorded by the aforementioned methodology.

In vivo sPD-1-15&15R@VNP-mediated therapy

To evaluate the effectiveness of combined sPD-1-15&15R@VNP and MWA therapy, Balb/c mice with subcutaneous CT26 tumors were randomly divided into five experimental groups. These groups were treated as follows when the tumor volume reached 100 mm³: group I received PBS alone, group II received MWA alone, group III received sPD-1@VNP + MWA, group IV received 15&15R@VNP + MWA, and group V received sPD-1-15&15R@VNP + MWA. Mice in groups III, IV, and V were intravenously injected with sPD-1@VNP, 15&15R@VNP, and sPD-1-15&15R@VNP at a dose of 2×10^6 CFU per mouse, respectively, while the other groups received an intravenous injection of PBS. Three days later, microwave therapy was performed on all groups except group I. The tumor growth and survival of mice were recorded by the aforementioned methodology. On day 7, one mouse from each group in the CT26-tumor-bearing model was randomly selected, and the tumor was collected for evaluation of the early-stage therapeutic efficacy using TUNEL and H&E staining.

In vivo experiment to block lymphocyte migration

To block the emigration of lymphocytes from secondary lymphoid organs, mice were i.v. injected with FTY720 (ENZO Life Sciences) one day prior to the MWA treatment and continued every other day at a dose of 20 μg per mouse.

In vivo sPD-1-15&15R@VNP-mediated therapy N1S1 orthotopic rat liver tumor model

Fifteen SD rats bearing N1S1 orthotopic tumors were divided into three groups and treated as below: group I, PBS; group II, MWA treatment; group III, MWA + RsPD-1-15&15R@VNP. These SD rats of group II were intravenously injected with RsPD-1-15&15R@VNP at day 0 at a dose of 2×10^7 CFU (200 μL), while these SD rats of groups II and III were subjected to MWA treatment at day 3. At day 0 before different treatments and 7, 14 days post different treatment, these rats were then subjected to a 3.0-T MRI imaging system for recording the tumor volumes (SIGNA Architect, GE Healthcare, Milwaukee, USA)) for recording the tumor volume.

Statistical analysis

All data are reported as the mean ± standard errors of the mean (SEM) or mean ± standard deviation (SD), as indicated. One-way or two-way analysis of variance (ANOVA) was typically carried out when three or more groups were compared, and when the test result was statistically significant ($p < 0.05$), multiple group comparisons were carried out by Tukey's post hoc test. Student's t test was carried out for two group comparisons. Statistical tests were performed with GraphPad Prism 9.0. The level of statistical significance was expressed as *$p < 0.05$, **$p < 0.01$, ***$p < 0.001$. Genes differential expression analysis was performed by DESeq2 R3.6.2 software between two different groups (and by edgeR R4.0.2 between two samples). The genes with the parameter of false discovery rate below 0.05 and absolute fold change ≥2 were considered differentially expressed genes, which were then subjected to enrichment analysis of GO functions and KEGG pathways. Bioinformatic analysis was performed using the OmicStudio tools at https://www.omicstudio.cn/tool.

Reporting summary

Further information on research design is available in the Nature Portfolio Reporting Summary linked to this article.

Data availability

The sequencing data of the transcriptomic analyses in this study are available from the Sequence Read Archive (SRA) Run Selector of the National Center Biotechnology Information (NCBI) database. SRA records are accessible with the following link: https://www.ncbi.nlm.nih.gov/sra/PRJNA1175425. The remaining data are available within the Article, Supplementary Information or Source Data file. Source data are provided with this paper.

References

1. Llovet, J. M. et al. Locoregional therapies in the era of molecular and immune treatments for hepatocellular carcinoma. *Nat. Rev. Gastroenterol. Hepatol.* **18**, 293–313 (2021).
2. Liang, P. et al. Percutaneous cooled-tip microwave ablation under ultrasound guidance for primary liver cancer: a multicentre analysis of 1363 treatment-naive lesions in 1007 patients in China. *Gut* **61**, 1100–1101 (2012).
3. Zaidi, N. et al. Laparoscopic microwave thermosphere ablation of malignant liver tumors: an analysis of 53 cases. *J. Surg. Oncol.* **113**, 130–134 (2016).
4. Qin, S. et al. The local efficacy and influencing factors of ultrasound-guided percutaneous microwave ablation in colorectal liver metastases: a review of a 4-year experience at a single center. *Int. J. Hyperth.* **36**, 36–43 (2019).
5. Livraghi, T., Meloni, F., Solbiati, L. & Zanus, G. Complications of microwave ablation for liver tumors: results of a multicenter study. *Cardiovasc. Interv. Radiol.* **35**, 868–874 (2012).
6. Mansurov, A. et al. Masking the immunotoxicity of interleukin-12 by fusing it with a domain of its receptor via a tumour-protease-cleavable linker. *Nat. Biomed. Eng.* **6**, 819–829 (2022).
7. Deckers, J. et al. Engineering cytokine therapeutics. *Nat. Rev. Bioeng.* **1**, 286–303 (2023).
8. West, E. E. et al. PD-L1 blockade synergizes with IL-2 therapy in reinvigorating exhausted T cells. *J. Clin. Investig.* **123**, 2604–2615 (2013).
9. Waldmann, T. A., Dubois, S., Miljkovic, M. D. & Conlon, K. C. IL-15 in the combination immunotherapy of cancer. *Front. Immunol.* **11**, 868 (2020).
10. Waldmann, T. A. & Tagaya, Y. The multifaceted regulation of interleukin-15 expression and the role of this cytokine in NK cell differentiation and host response to intracellular pathogens. *Annu. Rev. Immunol.* **17**, 19–49 (1999).
11. Stonier, S. W. & Schluns, K. S. Trans-presentation: a novel mechanism regulating IL-15 delivery and responses. *Immunol. Lett.* **127**, 85–92 (2010).
12. Dubois, S., Mariner, J., Waldmann, T. A. & Tagaya, Y. IL-15Ralpha recycles and presents IL-15 In trans to neighboring cells. *Immunity* **17**, 537–547 (2002).
13. Burkett, P. R. et al. Coordinate expression and trans presentation of interleukin (IL)-15Ralpha and IL-15 supports natural killer cell and memory CD8+ T cell homeostasis. *J. Exp. Med.* **200**, 825–834 (2004).
14. Lee, J. et al. IL-15 promotes self-renewal of progenitor exhausted CD8 T cells during persistent antigenic stimulation. *Front. Immunol.* **14**, 1117092 (2023).
15. Jansen, C. S. et al. An intra-tumoral niche maintains and differentiates stem-like CD8 T cells. *Nature* **576**, 465–470 (2019).
16. Guo, Y., Luan, L., Patil, N. K. & Sherwood, E. R. Immunobiology of the IL-15/IL-15Rα complex as an antitumor and antiviral agent. *Cytokine Growth Factor Rev.* **38**, 10–21 (2017).
17. Guo, J. et al. Tumor-conditional IL-15 pro-cytokine reactivates anti-tumor immunity with limited toxicity. *Cell Res.* **31**, 1190–1198 (2021).
18. Pabani, A. & Gainor, J. F. Facts and hopes: immunocytokines for cancer immunotherapy. *Clin. Cancer Res.* **29**, 3841–3849 (2023).

19. Melero, I., Castanon, E., Alvarez, M., Champiat, S. & Marabelle, A. Intratumoural administration and tumour tissue targeting of cancer immunotherapies. *Nat. Rev. Clin. Oncol.* **18**, 558–576 (2021).

20. Yuan, J. et al. Current strategies for intratumoural immunotherapy—beyond immune checkpoint inhibition. *Eur. J. Cancer* **157**, 493–510 (2021).

21. Forbes, N. S. Engineering the perfect (bacterial) cancer therapy. *Nat. Rev. Cancer* **10**, 785–794 (2010).

22. Gurbatri, C. R., Arpaia, N. & Danino, T. Engineering bacteria as interactive cancer therapies. *Science* **378**, 858–864 (2022).

23. Zhou, S., Gravekamp, C., Bermudes, D. & Liu, K. Tumour-targeting bacteria engineered to fight cancer. *Nat. Rev. Cancer* **18**, 727–743 (2018).

24. McNerney, M. P., Doiron, K. E., Ng, T. L., Chang, T. Z. & Silver, P. A. Theranostic cells: emerging clinical applications of synthetic biology. *Nat. Rev. Genet.* **22**, 730–746 (2021).

25. Zheng, J. H. et al. Two-step enhanced cancer immunotherapy with engineered Salmonella typhimurium secreting heterologous flagellin. *Sci. Transl. Med.* **9**, https://doi.org/10.1126/scitranslmed.aak9537 (2017).

26. Royo, J. L. et al. In vivo gene regulation in Salmonella spp. by a salicylate-dependent control circuit. *Nat. Methods* **4**, 937–942 (2007).

27. Hartsough, L. A. et al. Optogenetic control of gut bacterial metabolism to promote longevity. *eLife* **9**, https://doi.org/10.7554/eLife.56849 (2020).

28. Abedi, M. H. et al. Ultrasound-controllable engineered bacteria for cancer immunotherapy. *Nat. Commun.* **13**, 1585 (2022).

29. Chen, Y., Du, M., Yuan, Z., Chen, Z. & Yan, F. Spatiotemporal control of engineered bacteria to express interferon-γ by focused ultrasound for tumor immunotherapy. *Nat. Commun.* **13**, 4468 (2022).

30. Wang, W. et al. Systemic immune responses to irradiated tumours via the transport of antigens to the tumour periphery by injected flagellate bacteria. *Nat. Biomed. Eng.* **6**, 44–53 (2022).

31. Zheng, Jin et al. Two-step enhanced cancer immunotherapy with engineered Salmonella typhimurium secreting heterologous flagellin. *Sci. Transl. Med.* **9**, eaak9537 (2017).

32. Piraner, D. I., Abedi, M. H., Moser, B. A., Lee-Gosselin, A. & Shapiro, M. G. Tunable thermal bioswitches for in vivo control of microbial therapeutics. *Nat. Chem. Biol.* **13**, 75–80 (2017).

33. Zhang, C. et al. Production of α-ketobutyrate using engineered Escherichia coli via temperature shift. *Biotechnol. Bioeng.* **113**, 2054–2059 (2016).

34. Mortier, E. et al. Soluble interleukin-15 receptor alpha (IL-15R alpha)-sushi as a selective and potent agonist of IL-15 action through IL-15R beta/gamma. Hyperagonist IL-15 × IL-15R alpha fusion proteins. *J. Biol. Chem.* **281**, 1612–1619 (2006).

35. Su, L., Yu, L., Xu, C. & Wu, J. Extracellular expression of Thermobifida fusca cutinase with pelB signal peptide depends on more than type II secretion pathway in Escherichia coli. *J. Biotechnol.* **204**, 47–52 (2015).

36. Clairmont, C. et al. Biodistribution and genetic stability of the novel antitumor agent VNP20009, a genetically modified strain of Salmonella typhimurium. *J. Infect. Dis.* **181**, 1996–2002 (2000).

37. Zhao, Q. et al. Microwave ablation combined with attenuated Salmonella typhimurium for treating hepatocellular carcinoma in a rat model. *Oncotarget* **8**, 47655–47664 (2017).

38. Yu, J. et al. Percutaneous cooled-probe microwave versus radiofrequency ablation in early-stage hepatocellular carcinoma: a phase III randomised controlled trial. *Gut* **66**, 1172–1173 (2017).

39. Kim, H. J. & Cantor, H. CD4 T-cell subsets and tumor immunity: the helpful and the not-so-helpful. *Cancer Immunol. Res.* **2**, 91–98 (2014).

40. Chow, A., Perica, K., Klebanoff, C. A. & Wolchok, J. D. Clinical implications of T cell exhaustion for cancer immunotherapy. *Nat. Rev. Clin. Oncol.* **19**, 775–790 (2022).

41. Chen, J. et al. Salmonella flagella confer anti-tumor immunological effect via activating Flagellin/TLR5 signalling within tumor microenvironment. *Acta Pharm. Sin. B* **11**, 3165–3177 (2021).

42. Means, T. K., Hayashi, F., Smith, K. D., Aderem, A. & Luster, A. D. The Toll-like receptor 5 stimulus bacterial flagellin induces maturation and chemokine production in human dendritic cells. *J. Immunol.* **170**, 5165–5175 (2003).

43. Schmitt, S. et al. Fusion of bacterial flagellin to a dendritic cell-targeting αCD40 antibody construct coupled with viral or leukemia-specific antigens enhances dendritic cell maturation and activates peptide-responsive T cells. *Front. Immunol.* **11**, 602802 (2020).

44. Li, M. et al. Inhibition of acute leukemia with attenuated Salmonella typhimurium strain VNP20009. *Biomed. Pharmacother.* **129**, 110425 (2020).

45. Friedl, P. & Weigelin, B. Interstitial leukocyte migration and immune function. *Nat. Immunol.* **9**, 960–969 (2008).

46. Paley, M. A. et al. Progenitor and terminal subsets of CD8+ T cells cooperate to contain chronic viral infection. *Science* **338**, 1220–1225 (2012).

47. Miller, B. C. et al. Subsets of exhausted CD8(+) T cells differentially mediate tumor control and respond to checkpoint blockade. *Nat. Immunol.* **20**, 326–336 (2019).

48. Im, S. J. et al. Defining CD8+ T cells that provide the proliferative burst after PD-1 therapy. *Nature* **537**, 417–421 (2016).

49. Blackburn, S. D., Shin, H., Freeman, G. J. & Wherry, E. J. Selective expansion of a subset of exhausted CD8 T cells by alphaPD-L1 blockade. *Proc. Natl. Acad. Sci. USA* **105**, 15016–15021 (2008).

50. Siddiqui, I. et al. Intratumoral Tcf1(+)PD-1(+)CD8(+) T cells with stem-like properties promote tumor control in response to vaccination and checkpoint blockade immunotherapy. *Immunity* **50**, 195–211.e110 (2019).

51. Utzschneider, D. T. et al. T cell factor 1-expressing memory-like CD8(+) T cells sustain the immune response to chronic viral infections. *Immunity* **45**, 415–427 (2016).

52. Sun, Q. et al. BCL6 promotes a stem-like CD8(+) T cell program in cancer via antagonizing BLIMP1. *Sci. Immunol.* **8**, eadh1306 (2023).

53. Mandala, S. et al. Alteration of lymphocyte trafficking by sphingosine-1-phosphate receptor agonists. *Science* **296**, 346–349 (2002).

54. Xie, W. et al. Immune checkpoint inhibitors therapies in patients with cancer and preexisting autoimmune diseases: a meta-analysis of observational studies. *Autoimmun. Rev.* **19**, 102687 (2020).

55. Saxton, R. A., Glassman, C. R. & Garcia, K. C. Emerging principles of cytokine pharmacology and therapeutics. *Nat. Rev. Drug Discov.* **22**, 21–37 (2023).

56. Leonard, W. J. & Lin, J.-X. Strategies to therapeutically modulate cytokine action. *Nat. Rev. Drug Discov.* **22**, 827–854 (2023).

Acknowledgements

Author contributions

Conceptualization: Y.M.W., L.Z.F., and Z.L. Methodology: Y.M.W. and L.Z.F. Investigation: Y.M.W., B.L., Y.F.Y., C.T.G., K.W.W., N.H.L., Y.J.Z., M.Y.L., C.J.W., and Y.Z.Y. Supervision: L.Z.F. and Z.L. Writing—original

draft: Y.M.W., L.Z.F., and Z.L. Writing—review and editing: Y.M.W., L.Z.F., and Z.L.

Competing interests

The authors declare no competing interests.

Additional information

Supplementary information The online version contains supplementary material available at https://doi.org/10.1038/s41467-024-54883-x.

Correspondence and requests for materials should be addressed to Liangzhu Feng or Zhuang Liu.

Peer review information *Nature Communications* thanks the anonymous reviewer(s) for their contribution to the peer review of this work. A peer review file is available.

Reprints and permissions information is available at http://www.nature.com/reprints

Publisher's note Springer Nature remains neutral with regard to jurisdictional claims in published maps and institutional affiliations.